AN ABSTRACT OF THE THESIS OF

Dustin Kasparek for the degree of Master of Science in Nuclear Engineering presented on June 5th, 2019.

Title: Feasibility of Enrichment Measurements with a Pixelated CdTe HEXITEC Detector: A Comparison of Methods

Abstract approved:

Camille Palmer

The International Atomic Energy Agency (IAEA) is responsible for verifying the mass of elemental uranium in various forms (powders, pellets, scrap) as part of safeguards inspections at nuclear fuel fabrication facilities in support of the nuclear non-proliferation treaty. Current methods require in-field dissolution chemistry, which is time consuming and imposes operational challenges. A rapid, nondestructive assay method would streamline inspections. Pacific Northwest National Laboratory (PNNL) is developing a prototype spectral X-ray radiography (SpecX) nondestructive assay system for noninvasive material mass quantification of uranium-bearing powders. The current method used by the IAEA also provides the enrichment of the uranium-bearing powders while the SpecX system does not. The presented research explores the ability to measure ^{235}U enrichment using the SpecX system in order to meet the full capabilities of the current methodology. This research compares various methods of enrichment calculations utilizing spectroscopy and supported by Monte Carlo simulations. Out of the tested

methodologies, the Ratio method has shown promise for accurate enrichment calculations using the HEXITEC system. Future research will aim to confirm the accuracy of the method.

Feasibility of Enrichment Measurements with a Pixelated CdTe HEXITEC Detector: A Comparison of Methods

by

Dustin Kasparek

A THESIS

submitted to

Oregon State University

in partial fulfillment of
the requirements for the
degree of

Master of Science

Presented June 5th, 2019
Commencement June, 2019

Master of Science thesis of Dustin Kasparek presented on June 5th, 2019.

APPROVED:

Major Professor, representing Nuclear Engineering

Head of the School of Nuclear Science and Engineering

Dean of the Graduate School

I understand that my thesis will become part of the permanent collection of Oregon State University libraries. My signature below authorizes release of my thesis to any reader upon request.

Dustin Kasparek, Author

ACKNOWLEDGMENTS

This research was supported by the U.S. National Nuclear Security Administration (NNSA) Office of Nonproliferation and Arms Control (NPAC) within the U.S. Department of Energy (DOE) under Contract DE-AC05-76RL01830. DM Kasparek is supported by the Safeguards Internship Program sponsored by the NNSA's Office of International Nuclear Safeguards PNNL-28747.

I would like to thank my two advisors, Ben McDonald and Dr. Camille Palmer, for their constant counsel and guidance. Without them, this research would not have been finished in time. I would also like to thank Rick Wittman for his help modeling my system as well as applying his well-defined DRF to my simulated data. Lastly, I would like to thank the Nuclear Science and Engineering graduate support staff here at Oregon State University. They were extremely helpful every step along the way.

TABLE OF CONTENTS

TABLE OF CONTENTS (Continued)

LIST OF FIGURES

LIST OF FIGURES

LIST OF FIGURES

LIST OF FIGURES

LIST OF FIGURES

LIST OF FIGURES

LIST OF TABLES

LIST OF TABLES

LIST OF TABLES

LIST OF TABLES

1 Introduction

The International Atomic Energy Agency (IAEA) is responsible for verifying the mass of elemental uranium in various forms (powders, pellets, scrap) as part of safeguards inspections at nuclear fuel fabrication facilities in support of the nuclear non-proliferation treaty. Currently, this is performed with a destructive analysis method, known as COMPUCEA, that requires in-field dissolution chemistry, which is time consuming and imposes operational challenges. Pacific Northwest National Laboratory (PNNL) is developing a prototype spectral X-ray radiography (SpecX) nondestructive assay system for noninvasive material mass quantification of uranium-bearing powders. The proposed system would provide a rapid nondestructive quantification of total uranium mass for nuclear safeguards applications while offering a lower operation burden than is required with current methods [1]. The COMPUCEA method used by the IAEA also provides the enrichment of the uranium-bearing powders, while the SpecX system does not [7]. The presented research explores the ability to measure ^{235}U enrichment using the pixelated CdTe HEXITEC detector from the SpecX system in order to meet the full capabilities of the currently-implemented methodology. The research compares three methods of enrichment calculations utilizing spectroscopy, including the Fixed energy Response function Analysis with Multiple efficiencies (FRAM), the Ratio method and the Gamma Enrichment Measurements (GEM) method. Monte Carlo simulations are first verified against

experimental data, then used as a tool for generating simulated enrichment spectra to test the performance of the methods at broader range of enrichments. Statistical methods are used to evaluate whether or not the SpecX system is able to accurately and consistently measure ^{235}U enrichment.

1.1 IAEA

The IAEA was created in 1957 in response to the rise of nuclear technology and weapons. It was created with the aim to promote safe, secure and peaceful nuclear technology. In 1970 the Treaty on the Non-Proliferation of Nuclear Weapons (NPT) entered into force. This treaty has become the most widely adhered to treaty in the field of non-proliferation and disarmament, a total of 191 States have joined since its inception [2]. The IAEA has many responsibilities involving nuclear safeguards that has grown over time with the addition of the Additional Protocol (AP). The AP is a way of providing additional tools to the IAEA for verification in the form of facility access. In particular, it significantly increases the IAEA's ability to verify the peaceful use of all nuclear material in States with comprehensive safeguards agreements (CSA). As of December 2018, 134 States and Euratom have signed the AP agreements [4]. The roles and responsibilities of the IAEA have dramatically increased in the 60 years since its creation. This is a direct result of new States making safeguards agreements causing the number of nuclear facilities that require inspections to increase year after year.

In 2015 there were 1,286 nuclear facilities and locations outside fa-

cilities under IAEA safeguards, 2,118 in-field inspections totaling 13,248 calendar days, and almost 800,000 nuclear material accountancy reports were received. All of this was accomplished on a budget of €132.5 million plus an additional €43.3 million were provided in extrabudgetary contributions [5]. This could appear to be a large budget to some; however, when tasked with ensuring that none of the 1,286 facilities inspected by the IAEA are proliferating, this budget does not seem very large. It is for this reason that the IAEA has continually pushed towards innovating their technology to reduce overhead costs while retaining or improving measurement accuracy and precision.

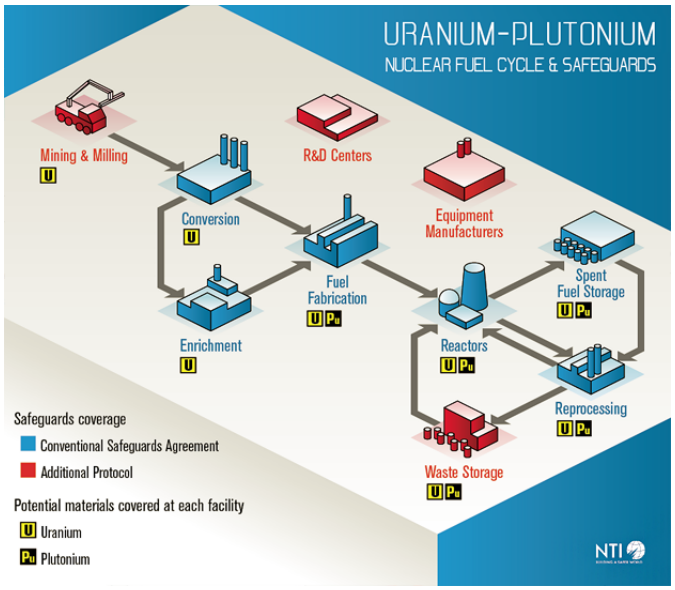

Figure 1: Graphic of the nuclear fuel cycle and the coverage resulting from safeguards. The coverage under the CSA are colored blue and the coverage under the AP are shown in red. [3]

This work is focused on IAEA verification inspections at nuclear fuel fabrication facilities. Fig. 1 above depicts the nuclear fuel cycle and the

associated safeguards coverage. In the middle of this image is nuclear fuel fabrication; this is where the fuel is pressed into pellets, sintered and shuffled into fuel rods for use at nuclear power facilities. This is a very important step in the fuel cycle as it is the last step that the fuel is accessible before the fuel is inserted into the reactor. After this point, the fuel becomes highly radioactive due to fission products and actinide production. For this reason, the IAEA has physical inventory verification (PIV) inspections at nuclear fuel fabrication facilities to verify the completeness and correctness of declared quantities. One of the measurements performed during these inspections verifies both the ^{235}U enrichment as well as the mass of elemental uranium in the form of liquids, powders, pellets or scrap. The current method that performs this task is called the Combined Procedure for Uranium Concentration and Enrichment Assay (COMPUCEA) [9].

1.2 COMPUCEA

COMPUCEA is an established safeguards-authorized portable analytical system that is capable of on-site bias defect verification measurements of uranium-bearing materials. Beginning in 2007, COMPUCEA has been routinely utilized by Euratom during PIV campaigns at European fuel fabrication plants [7]. It is utilized to measure in-field uranium concentration and ^{235}U abundance. The system is comprised of two parts, the first is an X-ray absorption-edge spectrometer used for the U elemental assay and the second is the gamma-ray spectrometer used for the ^{235}U enrichment determination.

The COMPUCEA system is portable and can travel between various sites. It is a destructive analysis (DA) method as samples (powder, scrap, pellets) are dissolved in solution prior to spectrometric measurements. However, if the sample is already in solution form, the COMPUCEA system is non-destructive analysis (NDA) method. The part of the system that assays the elemental uranium uses an L-edge densitometer, while Lanthanum (III) Bromide ($LaBr_3$) detectors are used to determine the ^{235}U enrichment assay. The additional infrastructure/supplies that are required for the system are as follows:

- Fume hood
- Portable densitometer
- Hot plate / Analytical balance
- NGSS (Next Generation Surveillance System)
- Nitric acid / de-ionized water
- Reference material for system calibration

In total, to prepare the samples, perform the measurements and analyze the results typically takes 3+ days in a standard schedule. These steps are carried out by a chemist and a NDA specialist [6]. The international target values (ITVs-2010) for measurement uncertainties in safeguarding nuclear material gives 0.28 and 0.45% for the combined relative standard deviations (RSD) of the uranium concentration and enrichment measurements with COMPUCEA, respectively [8].

To calculate the ^{235}U enrichment the COMPUCEA system uses an adapted version of the NaIGEM algorithm [7]. The NaIGEM algorithm was developed to improve upon ^{235}U enrichment measurements using a NaI detector [10]. GEM was modified in order to be capable of analyzing the spectra collected using the $LaBr_3$ detectors in the COMPUCEA system. The NaIGEM algorithm relies on measuring the 185.7 keV peak from ^{235}U on non-infinitely thick samples. The net peak area is determined using a calculated detector response with a non-linear least square fitting procedure. Using this methodology along with careful sample prep, the COMPUCEA system is able to attain RSD values of 0.45% on the ^{235}U enrichment calculation [8].

1.3 SpecX System

Pacific Northwest National Laboratory (PNNL) has developed a prototype spectral X-ray radiography (SpecX) nondestructive assay system for non-invasive material mass quantification of uranium-bearing powders [6]. The system includes an X-ray generator, a Cadmium Telluride (CdTe) spectroscopic detector, a sample to measure and a laptop for analysis; a general schematic of the system can be seen in Fig. 2.

The system is able to measure the elemental uranium concentration by observing the X-ray transmission around the K-edge, which for uranium is at 115.6 keV [13]. The X-ray generator produces a bremsstrahlung spectrum with a 160 keV endpoint, which is attenuated by the uranium sample and

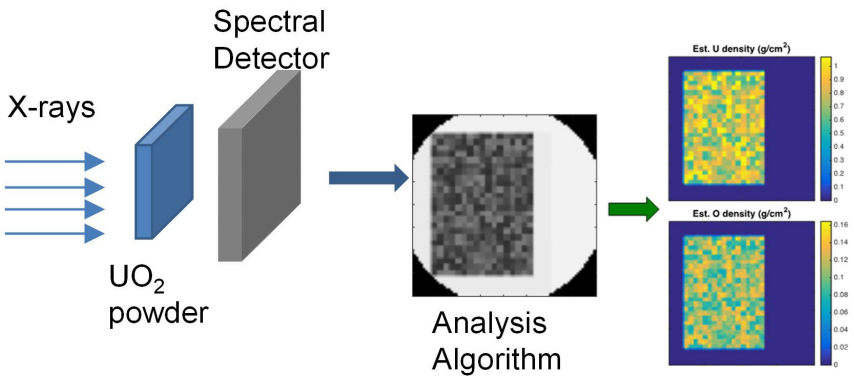

Figure 2: Depiction of the spectral X-ray (SpecX) radiography assay system and algorithm.

measured on a pixelated CdTe spectroscopic detector. Utilizing Beer's law:

$$d(\boldsymbol{\rho}, E_{bin,l}) = \int_0^\infty S_l(E)\phi_0(E)\exp\left[-\sum_k \mu_k(E)\rho_k\right]dE \tag{1}$$

Where d is the detector output for each energy bin and S_l is the energy-dependent bin sensitivity of energy bin l. The X-ray flux at the image plane is ϕ, ϕ_0 is the unattenuated flux, μ_k is the mass attenuation coefficient of the k'th material and ρ_k is the areal density in a given pixel. The density vector $\boldsymbol{\rho}$ indicates that the transmitted flux is dependent on a vector of any number of materials between the X-ray source and the detector. Using Beer's law one can solve the forward problem of using the known assay-system parameters to generate an expected output from the spectral X-ray radiography system. However, in the case of an unknown output, a more applicable problem is to use the data output from the radiography system to determine the material composition. This inverse problem is the calculation performed in the SpecX

algorithm as depicted in Fig. 3 [12].

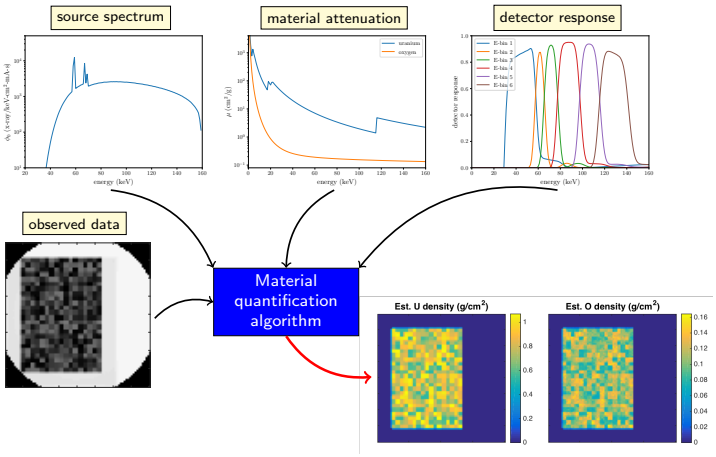

Figure 3: Depiction of the spectral X-ray (SpecX) radiography assay system [6].

It can be observed in Fig. 3 the X-ray generated source spectrum, the material attenuation spectrum and the detector response function are all components that feed into SpecX's material quantification algorithm. The output from the algorithm is the image shown in the bottom right of Fig. 3, where the dark blue represents the unattenuated region and the mixed-color squares represent the material mass estimation for either the uranium (left) or oxygen (right). Initial results indicate a repeat measurement uncertainty better than 1%. Ongoing refinements to the system and algorithm aim to increase this performance level. Therefore, the SpecX system is able to non-destructively estimate the uranium mass within reasonable error. The current approach to acquire, process, and analyze a sample takes approximately thirty minutes with a high-powered computer. The system shows promise in rapidly and accurately assaying the elemental uranium. However, the COM-

PUCEA system used by Euratom and the IAEA provides both the elemental uranium assay and the ^{235}U enrichment. Hence, the purpose of this thesis is to make the SpecX system complementary by offering a similar enrichment assay capability as the COMPUCEA system.

1.4 Enrichment Measurements

The need to quantify the ^{235}U enrichment throughout the nuclear fuel cycle is valuable to the nuclear industry. For example, a nuclear fuel manufacturer selling their product must be able to prove that their fuel is of a certain enrichment. For the IAEA, they must measure the enrichment in order to verify that it matches what the inspected facility declares. Over the decades the method of calculation has evolved to offer higher sensitivity, a more rapid analysis turnaround, and a robustness to sample variations and measurement conditions (e.g. container wall thickness) [9].

Since the late 1990s, ^{235}U enrichment quantification has been achieved primarily through the means of radiation spectroscopy. Several different detector types have been utilized, including High-Purity Germanium (HPGe), Low-Energy Germanium (LEGe), sodium iodide (NaI), Lanthanum (III) Bromide ($LaBr_3$), and also CdTe/CZT [10, 14–20, 27]. All of these detectors have associated strengths and weaknesses. NaI detectors are inexpensive and have high intrinsic efficiencies, but have relatively poor energy resolution. HPGe/LEGe detectors have very fine energy resolution which allows for more accurate measurements, but generally require cooling and are more

expensive. Lastly, CdTe/CZT falls somewhere in the middle in terms of cost, energy resolution and intrinsic efficiency. CdTe/CZT is able to operate at room temperature due to having a bandgap energy of 1.52 eV , providing an advantage over HPGe detectors. For these reasons, algorithms to calculate ^{235}U enrichment have been developed for each of these respective detectors. NaIGEM is used for NaI detectors, but has also been modified to work with $LaBr_3$/CZT detectors for the COMPUCEA system [14]. Whereas, FRAM was developed for HPGe detectors, but can be modified to analyze CdTe detector due to their similar energy resolution [15]. However, the detector response functions are different due to low-energy hole-tailing in CdTe detectors.

The objective of the research is to determine the viability of using the HEXITEC CdTe detector to accurately measure ^{235}U enrichment. A total of six UO_2 pellet samples are acquired for testing. The uranium samples are then processed using seven different parameter sets. Three methods were chosen to evaluate the HEXITEC's ability to measure ^{235}U enrichment based on their availability and suitability. The FRAM, Ratio and GEM methods are tested on each of the parameter sets to determine the optimal parameters [10, 15, 18]. The accuracy of the three methods are quantified based on mean percent difference between the calculated and known enrichments as well as the mean percent residual standard deviations (RSD). The experimental system is modeled using Monte Carlo N-Particle version 6.2 (MCNP6.2) and validated using the measured data. The output spectra from MCNP6.2 are

applied to a detector response function (DRF) in FORTRAN to produce realistic CdTe detector results. After the simulated results match reasonably well to the measured results, new spectra can be generated with enrichments beyond what is available. This allows for the ability to test the accuracy of the three methods on enrichments that were not measured. Ultimately a conclusion will be made about the HEXITEC detector's ability to yield accurate ^{235}U enrichment calculations.

2 Equipment and Methods

The HEXITEC V2 detector system contains an 80 x 80-pixel CdTe array with 250 μm pitch and 1 mm thickness (Quantum Detectors, UK) [21, 22]. The readout electronics have been flip-chip bonded to the application-specific integrated circuits (ASICs), which reads out the pixels in a frame mode up to 10,000 frames per second [22]. The detector is operated at 200 Hz frame rate for the uranium enrichment measurements and 8 kHz frame rate during detector characterization. The detector is typically operated in its high gain mode, allowing for energy sensitivity between 2-200 keV with a default channel width of 0.25 keV, the channel width is altered for uranium enrichment measurements. The detector has a nominal full-width at half-maximum (FWHM) of 750 eV at 60 keV. To build a robust detector model several key features must be accurately determined: the energy calibration, charge sharing effects, spectral hole-tailing, and the intrinsic efficiency response for each

of the 6400 pixels.

2.1 Detector Characterization

2.1.1 Energy Calibration

A precise energy calibration is necessary for quantitative analysis. The uranium spectra used in the analysis are a result of summing pixel spectra illuminated by the uranium source. Therefore, poorly-calibrated pixels will cause peak broadening in the summed pixel spectrum. Further, the accuracy of the enrichment calculation from the algorithms is directly dependent on uranium peaks arising at their expected energies. The energy calibration used three radioisotopes: ^{241}Am, ^{57}Co, and ^{133}Ba, making use of their four high-yield lines at 31.0, 59.5, 81.0, and 122.0 keV. This allows for a robust energy calibration spanning most of the energy range of the detector and the uranium peaks of interest between 90-100 keV. The source activities were 0.498, 0.068, and 0.850 mCi respectively and were measured at a 10 cm source-to-detector distance, as seen in Fig. 4. The acquisition times were 148, 115, and 185 minutes respectively.

The peak finding algorithm performed continuous wavelet (Ricker wavelet or Mexican hat wavelet) transforms on individual pixel spectra to identify ridge lines which were then correlated to spectral peaks [23]. The true peak locations used in the calibration were determined using an automated 3-point quadratic fit at each photopeak. Each of the 6400 pixel spectra were

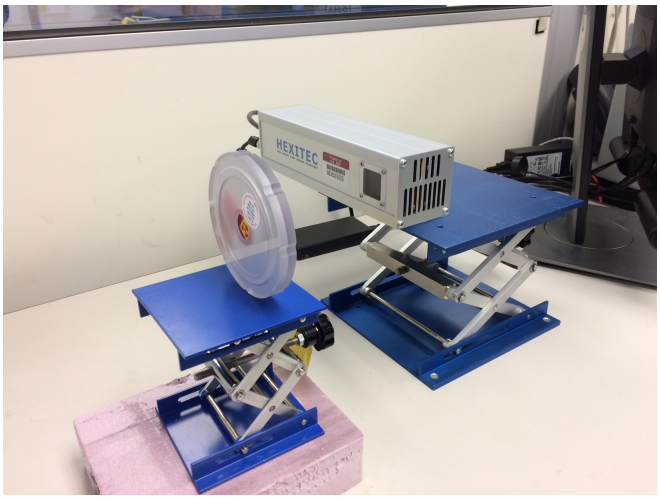

Figure 4: The experimental setup for the energy calibration measurements. Shown is the ^{241}Am (0.498 mCi) source at a 10 cm stand-off distance.

subsequently fit using a quadratic energy calibration over the four peaks. This results in an energy calibration equation $y = ax^2+mx+c$ which converts channels (x) into energy (y). Each pixel has its own a, m and c parameters. The pixel-by-pixel energy calibration is performed in an automated fashion, with minimal user input.

2.1.2 Charge Sharing

The HEXITEC's small pixel size means that a significant number of photon interactions will produce charge that is shared across neighboring pixels. These events must either be accurately modeled or removed to create a high-fidelity model of the detector. In normal operating conditions the number of events that will experience charge sharing exceeds 35% for the HEXITEC system [21]. The charge sharing effect is dependent on the photon energy

and interaction depth and can be affected by other processes such as carrier diffusion, repulsion, fluorescence and Compton scattering [21]. Due to low hole mobility within CdTe, interactions that occur close to the cathode will yield the best performance in terms of full charge collection in a single pixel [24].

There are two main methods implemented with HEXITEC post-processing software used to mitigate the effects of charge-sharing: charge sharing discrimination (CSD) and charge sharing addition (CSA) [21]. If no charge sharing corrections are applied the data is considered to be "raw", and may include spectra with many partial energy deposition events. The HEXITEC system records the energy deposition recorded in each pixel for every frame. This allows for event screening to ensure no charge-shared events are added to the spectra. In each frame, the pixels are scanned for event clusters that are suspected of charge sharing (i.e., neighboring pixels with signal above some threshold). In the CSD algorithm these events are thrown away. Alternatively, in the CSA algorithm these events are summed and placed at the pixel location that has the largest contribution, but only if they do not exceed detector's maximum energy (200 keV). Further, the number of pixels that are scanned in all directions, centered on the primary event, can be set to either 1 or 2. This forms a scanning grid around the primary event of dimensions 3x3 pixels or 5x5 pixels, this can be seen in Fig. 5.

The CSA approach is chosen in cases where net counts are more

important than spectral resolution, but can cause new peaks to appear due to errors in the summation process. The CSD approach is superior in preserving spectral features, e.g. an optimal FWHM, but has a reduced efficiency. Both techniques are explored in this research.

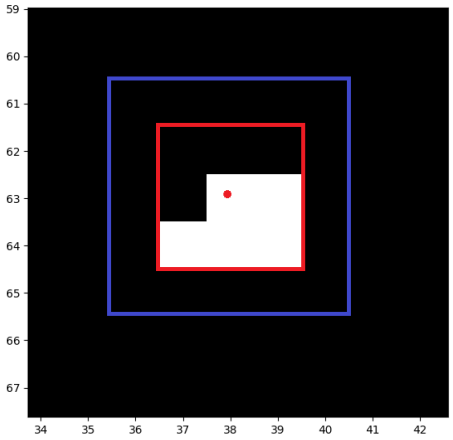

Figure 5: Depiction of a cluster of events within a frame, labeled as white squares, centered on the red dot. The 3x3 grid is shown as a red box and the 5x5 grid is shown as a blue box.

An additional post-processing technique used in the HEXITEC system is next frame correction (NFC) [21]. The NFC method looks for events that take place in the same pixel over two consecutive frames. If this condition occurs, then both events are removed. The NFC technique helps correct for events that occur near the end of a frame where the charge is not fully measured in the initial frame.

The CSD/CSA and NFC methods help to resolve artifacts that occur due to events that have charge shared among pixels or frames, thereby simplifying subsequent detector response modeling and increasing spectroscopic performance.

2.1.3 Detector Stability

Semiconductor detector crystals and their readout electronics are sensitive to temperature. Temperature fluctuations can cause a higher number of noise events to occur, as well as bias voltage drifts. During operation carrier trapping/detrapping at deep acceptor levels can cause polarization of the crystal [26]. This is overcome by performing a bias voltage refresh once every 60 seconds [25].

The CdTe crystal in the HEXITEC system is intended for room temperature operation. However, during detector operation the crystal, along with the electronics, will begin heating which can cause spectral degradation. This is observed primarily as peak broadening. To combat this, low-noise Peltier coolers are used and controlled using the HEXITEC's ASIC with an accuracy of ± 0.1 °C. The normal operating temperature for the detector is set to 18 °C. However, small temperature fluctuations are also problematic for the enrichment calculation algorithms, as the broadened peaks will result in an over-estimation of photopeak counts.

The detector stability was determined by observing the photopeak counts for the sum of all pixels over a period of time much longer than typical operations. A 0.498 mCi ^{241}Am source was used and was counted for ten minutes at a source-to-detector distance of 10 cm. This source was chosen due to its primary gamma line at 59.5 keV, which is in a high-efficiency energy region for this detector and it is far removed from other spectral features. This allows for simple peak finding/fitting to be performed in the analysis.

The stability metric used is the relative deviation from the mean photopeak counts.

$$D_{rel} = \frac{(x - \mu_x)}{\mu_x} * 100\% \tag{2}$$

Here, x is the photopeak counts for a ten-minute acquisition and μ_x is the mean photopeak counts over all acquisitions. The total photopeak counts were calculated by summing all counts 5 keV below and 1 keV above the photopeak, without background subtraction. A total of 13 ten-minute acquisitions were used for the stability analysis. Each acquisition was processed using both the CSD and NFC methods.

2.2 Sample Measurement

An important step in the feasibility analysis for the HEXITEC detector is the acquisition of the data that is used in each of the methods. The measurement campaign spanned a two week period in August of 2018. The laboratory where the measurements occurred is a "high-gamma activity lab", meaning background subtraction bears heavy importance. Therefore, a 12-hour background was acquired on the first and last day of measurements to ensure that the high background is accounted for in the data. In addition to subtracting the background, a ring of lead bricks were setup around the detection system to reduce the overall background, as shown in Fig. 6.

There were a total of eight uranium samples measured, ranging from $0.72\% \rightarrow 4.7\%^{235}$U . Six of these samples were in the form of uranium pellets,

while the remaining two samples were uranium pellet "slices". The pellet slices are former uranium pellets that were subsequently cut at a depth of 1 mm, making them very thin cylinders. Information regarding the data acquired over the measurement campaign can be found in Table 1.

Figure 6: Photo of the experimental setup for the uranium enrichment measurements, highlighting the lead brick enclosure.

Table 1: Measurement conditions for the eight uranium oxide samples.

Enrichment (%)	Acq. Time (Hours)	Form	S-D Distance (cm)
0.72	4	Pellet	3.18
2.6725	4	Pellet	3.18
3.2	4	Pellet	3.18
3.8862	4	Pellet	3.18
3.8862	4	Slice	3.18
4.15	4	Slice	3.18
4.4308	4	Pellet	3.18
4.7	4	Pellet	3.18

In Table 1, enrichment is the ^{235}U enrichment percentage (given with

Figure 7: Photo of the S-D distance of 1.25 inches (converted to 3.175 cm in Table 1).

the same number of significant figures provided), acq. time is the acquisition live time in hours, form denotes either a pellet or slice, and s-d distance is the source-detector distance in cm. Acquisition time and source-detector distance were kept constant across all samples, allowing for direct comparison. A tungsten collimator with dimensions 5 cm (width) x 7 cm (height) x 1.25 cm (thickness) and hole diameter 1 cm is placed directly in front of the detector as seen in Fig. 8. The collimator is added to produce a narrow beam, characterized as "good" geometry. In Fig. 8 it can be observed that the uranium pellet being measured is double-bagged. The plastic bags are thin enough such that there is negligible attenuation of the uranium signal.

All eight samples were collected for four hours and subsequently processed using either the CSA or CSD algorithm in combination with the NFC algorithm. These data were processed in a number of different configura-

tions, summarized in Table 2, to examine which combination yields the most accurate end result.

Figure 8: Photo of the experimental setup for the uranium enrichment measurements, highlighting tungsten collimator.

2.3 Enrichment Analysis Algorithms

2.3.1 FRAM Method

The Fixed energy, Response function Analysis with Multiple efficiencies, or FRAM, was developed by the Safeguards Science and Technology (SST) group at the Los Alamos National Laboratory (LANL). FRAM is a γ-ray isotopic analysis code developed to measure a wide range of plutonium and uranium samples [27]. The essence of γ-ray isotopic analysis relies upon relating photopeak areas to isotopic activity, which is then translated to isotopic fractions. The isotopic fractions are the ^{235}U enrichment measurements we

wish to calculate. Measured uranium samples typically contain three main isotopes ^{238}U, ^{235}U and ^{234}U, each contributing photopeaks to the measured γ-ray spectrum. The expression for the photopeak count rate from a particular γ-ray can be written as:

$$C(E_j^i) = \lambda^i \times N^i \times BR_j^i \times \varepsilon(E_j) \tag{3}$$

where:

$C(E_j^i)$ = photopeak count rate of gamma ray j with energy E_j emitted from isotope i,

λ^i = decay constant of isotope i, $\lambda^i = \ln 2 \; / \; T_{1/2}^i$, where $T_{1/2}^i$ is the half life of the isotope i,

N^i = number of atoms of isotope i,

BR_j^i = branching ratio (gamma rays/disintegration) of gamma ray j from isotope i,

$\varepsilon(E_j)$ = total efficiency for photopeak detection of a gamma ray with energy E_j. This includes detector efficiency, geometry (solid angle), sample self-absorption, and attenuation in packaging and materials between the sample and the detector.

If one wishes to calculate the atom ratios of two different isotopes one can manipulate Eq. 3:

$$\frac{N^i}{N^k} = \frac{C(E_j^i)}{C(E_l^k)} \times \frac{T_{1/2}^i}{T_{1/2}^k} \times \frac{BR_l^k}{BR_j^i} \times \frac{RE(E_l)}{RE(E_j)} \tag{4}$$

Where, RE is the relative efficiency at a specific γ-ray energy for isotope i or k. Using Eq. 4. one can calculate the atomic ratio of ^{235}U to ^{238}U i.e. the uranium enrichment. In this form, the half lives, $T_{1/2}$, and the branching ratios, BR, are known nuclear data. The relati‘ve efficiencies with respect to energy can either be experimentally found for a specific detector, however using Eq. 4 one only needs to know the ratio of the relative efficiency. For photopeaks that are close to each other in the spectrum e.g. $E_l \approx E_k$, the relative efficiencies will not vary by a meaningful amount e.g. $\frac{RE(E_l)}{RE(E_k)} \approx 1$. Lastly, the photopeak areas for each γ-ray from each isotope is calculated using the FRAM algorithm. Using the prior information and Eq. 4 one can calculate the atomic ratios for any sample. Specifically, this technique can be used to calculate the ^{235}U enrichment of various samples.

In order to obtain an accurate photopeak area, FRAM needs specific information such as the γ-ray energy, the relative efficiency at that energy, a valid DRF and knowledge of the FWHM variation with energy. FRAM V5.2 is pre-loaded with all necessary information regarding γ- and X-rays in the 50-210 keV range that are resultant from uranium and used to calculate the enrichment, as seen in Fig. 9. This information is utilized along with the detector crystal type to create an efficiency curve. FRAM V5.2 contains default DRF parameters for HPGe as well as CdTe as seen in Fig. 10. The FWHM energy dependence is also pre-loaded for HPGe and CdTe detectors. The above-mentioned parameters can all be manipulated within the FRAM graphical user interface (GUI) to provide a more accurate representation of

the user's specific system.

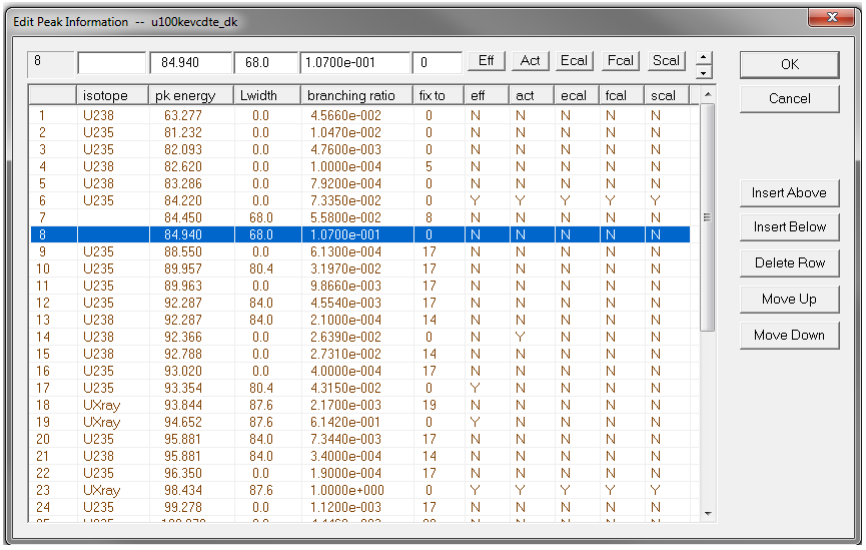

Figure 9: Depiction of the peak information listed in FRAM. The user is free to change all parameters, including whether or not each peak will be used in the internal calibrations.

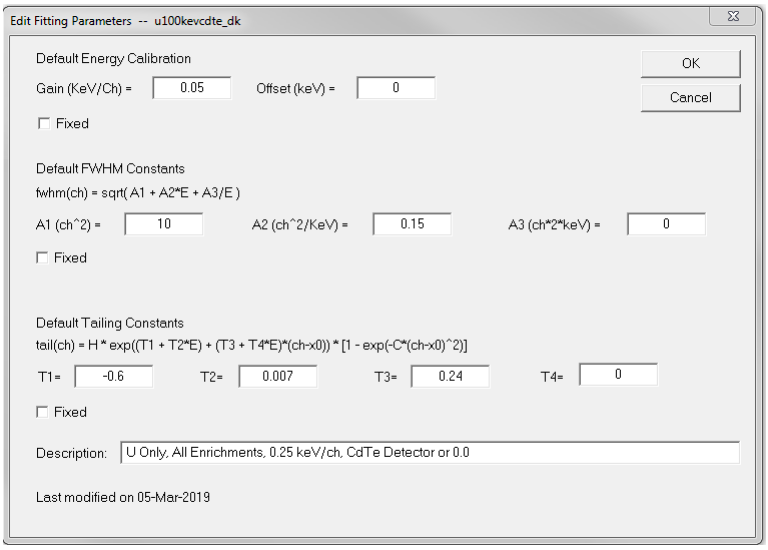

Figure 10: Depiction of the peak fitting parameters listed in FRAM, the user is free to change all parameters.

The FRAM algorithm performs a peak fitting process using the DRF

specified through adjusted parameters in the GUI, shown in Eqs. 5-7 below:

$$FWHM(E) = \sqrt{\left(A_1 + A_2E + \frac{A_3}{E}\right)} \tag{5}$$

$$Y(J) = H\exp\left(\alpha(J - x_0)^2\right) + Tail(J) \tag{6}$$

$$\begin{aligned} Tail(J) &= H \times \exp\Big[(T_1 + T_2E) + (T_3 + T_4E) * (J - x_0)\Big] \\ &\quad \times\Big[1 - \exp(-0.4\alpha(J - x_0)^2)\Big] \end{aligned} \tag{7}$$

Here, E represents energy in keV, $A_1 -> A_3$ are FWHM parameters with units $E^2, E^2/keV, E^2 * keV$ respectively, $Y(J)$ is the net count in channel J, H is the peak height at the peak centroid x_0, $\alpha = 2.77259/FWHM^2$ and is the peak width parameter, and $T_1 -> T_4$ are tailing parameters and are unitless. It should be noted that T_4 is set to zero in practice, which reduces the number of unknowns in Eq. 7 to three. After all initial parameters are set, FRAM has all the necessary information to calculate the shape of a gamma-ray peak at any location in the spectrum using a weighted least-squares iteration method.

To estimate the ^{235}U enrichment using FRAM, one can simply use the GUI's "Analyze" function within the "Measure" tab; the "Analyze" window is shown in Fig. 11. FRAM accepts spectra files in the forms of Canberra S100, Canberra CAM, IAEA MMCA, and ASCII. The IAEA MMCA format

was used for all data files with file extension ".spe". After clicking "OK" in Fig. 11 the FRAM code will analyze the input spectrum and compile all results in less than few seconds. The user is then given the option of viewing the "Short Result", "Med Result" or "Long Result", where each step yields additional information about the analysis.

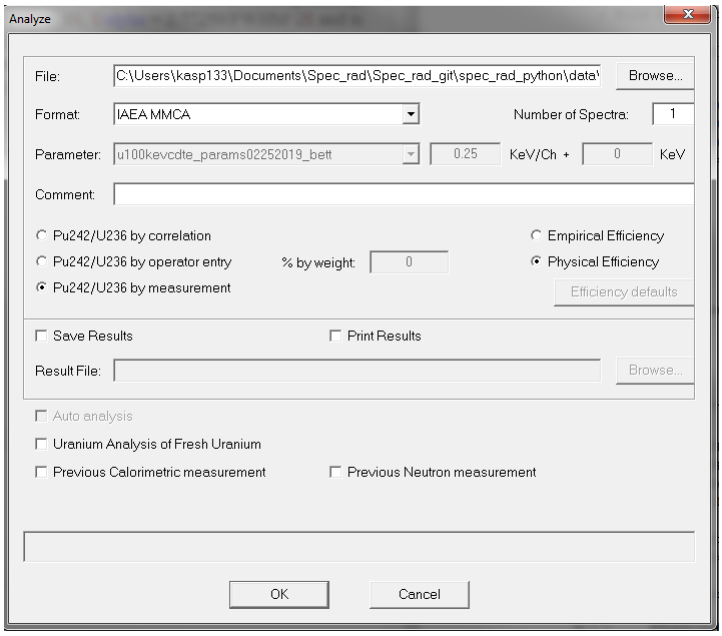

Figure 11: Depiction of the "Analyze" window in FRAM.

Fig. 12 shows an example of a "short" result from FRAM. The calculated enrichment results are highlighted with a red box. The mass %, sigma, and %RSD are provided for uranium isotopes ^{234}U, ^{235}U, ^{236}U, and ^{238}U. The mass % values will be used for the comparison of analysis methods. The sigma values are the absolute uncertainty representing one standard deviation propagated from counting statistics, which closely represents

the standard deviation that is observed from repeated measurements. The %RSD is calculated using $\%RSD = \frac{sigma}{mass\%} * 100\%$, which is different than how the IAEA calculates %RSD. Lastly, the percent difference between the calculated FRAM enrichment and the known enrichment is calculated using $\%Diff. = \frac{Measured - Expected}{Expected} * 100\%$.

```
********************************************************************************
PC FRAM (5.2)     Isotopic Analysis     09-Mar-2019 12:24:14
(Fixed energy Response function Analysis with Multiple efficiencies)
Operator ID:

spectrum source:  ~Enrich\CSA1\BW_250eV\Bkgsub\Only_ROI\enat_csa1_250eV_bkgsubROI2_1.spe
spectrum date:  09-Mar-2019 12:24:14
live time:  0 s
true time:  0 s
num channels:  801

parameter set:  u100kevcdte250 (Auto 0) (2019.02.20 17:22)
     U Only, All Enrichments, 0.25 keV/ch, CdTe Detector
    Physical Efficiency,  Gain 0.25 keV/ch, Offset 0 keV
comment:
********************************************************************************
***No peaks in region (330,343)
***No peaks in region (736,750)
***Invalid FWHM for peak 34
***Not enough peaks to calculate FWHM - will use defaults.
***Failed to calculate FWHM - will use defaults
***Failed to calculate tail - will use defaults.
********************************************************************************
at    84.220 keV, centroid =    343.000 [   670.760 < ? <    676.760]
at   185.715 keV, centroid =    750.000 [  1480.720 < ? <   1490.720]
at    84.220 keV, tail fraction =  25.87 [? <  10.00]
at   185.715 keV, tail fraction =  30.77 [? <  20.00]

                              (Measure)

             U234      U235      U236      U238
mass%      0.0187    0.6771    0.0000   99.3042
sigma      0.1040    0.7512    0.0000    0.7647
%RSD      >99.99%   >99.99%   >99.99%     0.77%

%TotPwr    75.76      0.91      0.00     22.33

Specific Power (W/gU):    (     0.0445 +/-     0.1875)e-006  (>99.99%)

Relative mass (Uxray / U):    4.400e-002  ( 44.54%)
********************************************************************************
```

Figure 12: Depiction of a "short" result from the FRAM code with the calculated enrichment highlighted with a red box.

The six samples were processed using seven different sets of processing parameters in order to explore which would yield the most accurate results. The variations in parameter settings can be observed in Table 2. The region of interest (ROI) used in parameter sets 4-7 is discussed in detail in Sec 3.2. The same seven parameter sets are used in all subsequent analysis

within FRAM, the ratio method and GEM.

Table 2: Parameter information used to process the six uranium samples.

Parameter Set	Bin Width (eV)	Charge Sharing Grid	Charge Sharing Algorithm	Background #	ROI (y/n)
1	250	3x3	CSA	2	n
2	50	3x3	CSD	1	n
3	50	3x3	CSA	NONE	n
4	250	3x3	CSA	1	y
5	250	3x3	CSA	2	y
6	250	3x3	CSD	1	y
7	250	3x3	CSD	2	y

2.3.2 Ratio Method

The ratio method is a method for calculating uranium enrichment using only the self-fluorescence X-rays and the 92^* γ-rays in the $90 - 100$ keV spectral region [18]. This is beneficial for the HEXITEC detector as this region lies directly in the middle of its measurable energy range where it has an intrinsic efficiency nearing 100%. The four peaks used in this form of analysis are shown in Table 3. Here the 92.4 and 92.8 keV peaks are an almost-real doublet and will further be referred to as a single 92^* peak. These γ-rays are both products of the interaction $^{238}U(\alpha) \rightarrow ^{234} Th(\gamma)$ i.e. the 92^* peak is dependent upon the number of ^{238}U atoms. The two other peaks used in the ratio method are the 94.65 and 98.43, K_{α_2} and K_{α_1} self-fluorescence X-rays respectively. The yield of these two peaks are dependent upon the number of

U atoms as well as the number of high-energy γ-rays passing by the U atoms that are above the self-excitation threshold.

Table 3: Table containing information about the energy, formation process and quantum yield of the four uranium peaks used in the ratio method [20]. The * represents the relative quantum yield.

Energy (keV)	Formation Process	Quantum yield (%)
92.37	$^{238}U(\alpha) \rightarrow^{234} Th(\gamma)$	2.52
92.79	$^{238}U(\alpha) \rightarrow^{234} Th(\gamma)$	2.50
94.65	Self-excitation of $UK\alpha_2(X)$	61.6*
98.43	Self-excitation of $UK\alpha_1(X)$	100*

However, measuring the net peak counts in this region is not as simple as calculating the peak area and subtracting the background. The uranium spectrum has other peaks in this region at 93.020, 93.844, 95.881, and 96.350 keV with branching ratios 0.004, 0.212, 0.0768, and 0.0019% respectively. If these peaks are unaccounted for, the peak areas of interest will be incorrect. Therefore, a spectrum de-convolution must be used in this region of the spectrum to isolate the peaks of interest. The spectrum de-convolution uses Eq. 7 (Sec. 2.3.1) to fit the data in each region according to the known peak locations and branching ratios, done within FRAM's analysis procedure. The results can be observed either as a plot or table, as shown in Figs. 13, 14.

Fig. 13 depicts the measured data as blue dots and the fit for each peak in the region as red lines, and lastly the sum of all individual fits is shown as a solid blue line. The quality of fit for the 90-100 keV region is visually inspected. In Fig. 14 the fit statistics are shown in detail. Importantly,

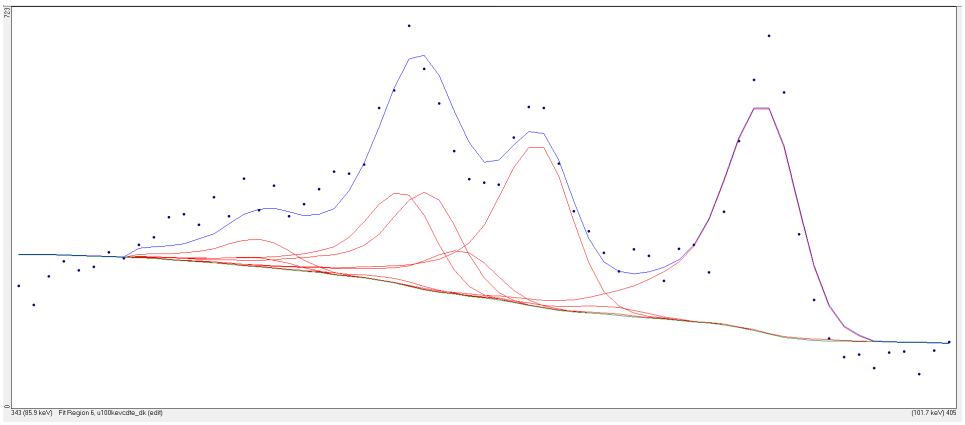

Figure 13: Depiction of 90-100 keV region of a 2.67% enriched sample with FRAM's summed fit shown as a blue line and the each peak fit's contribution shown as red lines, the original data is shown as blue data points.

region 6 from channel 351 to 399 (88.000 keV to 100.000 keV)

total net counts = 9253.
Qfit = 4.232e+000 R**2 = 0.81562 Cond = 2.837e+000

pk	isotope	energy	centroid	fwhm	tamp	tslp	area	% rsd	fn	factor
9	U235	88.550	353.541	4.825	1.020	0.240	6	38.15%	2	0.0107
10	U235	89.957	359.101	4.847	1.030	0.240	364	38.15%	2	0.6177
11	U235	89.963	359.125	4.847	1.030	0.240	112	38.15%	2	0.1907
12	U235	92.287	368.309	4.883	1.047	0.240	59	38.15%	2	0.1005
13	U238	92.287	368.309	4.883	1.047	0.240	9	13.34%	1	0.0079
14	U238	92.366	368.621	4.884	1.048	0.240	1174	13.34%	1	1.0000
15	U238	92.788	370.289	4.891	1.051	0.240	1240	13.34%	1	1.0557
16	U235	93.020	371.206	4.894	1.052	0.240	5	38.15%	2	0.0091
17	U235	93.354	372.525	4.899	1.055	0.240	590	38.15%	2	1.0000
18	Uxray	93.844	374.462	4.907	1.059	0.240	7	11.73%	3	0.0034
19	Uxray	94.652	377.655	4.919	1.065	0.240	2176	11.73%	3	1.0000
20	U235	95.881	382.512	4.938	1.074	0.240	110	38.15%	2	0.1860
21	U238	95.881	382.512	4.938	1.074	0.240	17	13.34%	1	0.0147
22	U235	96.350	384.365	4.945	1.077	0.240	3	38.15%	2	0.0049
23	Uxray	98.434	392.687	4.976	1.093	0.240	3088	7.25%	4	1.0000
24	U235	99.278	395.834	4.989	1.100	0.240	18	38.15%	2	0.0303

Figure 14: Depiction of the table of fit statistics output from FRAM for the 2.67% enriched sample.

the number of peaks are shown along with their associated peak areas and %RSD. With this information, the ratio method can then be implemented.

The name "ratio method" comes from the fact that the uranium enrichment is being calculated using two ratios of peak areas, $\frac{I_{94}}{I_{92^*}}$ and $\frac{I_{98}}{I_{92^*}}$, where I represents net counts. These two ratios are shown to increase linearly with ^{235}U enrichment [18, 20]. Therefore, a calibration curve can be

constructed simply by measuring several uranium samples of different enrichments and fitting their peak ratios with a linear line, $y = mx + b$. Here, y is the declared ^{235}U enrichment, m is the slope of the fitted line, x is the measured peak ratio, and b is the intercept of the fitted line. The quality of fit for the calibration equation is measured based on the R^2 coefficient. Further, to calculate the enrichment of a subsequent sample, one can measure the two peak ratios and utilize their established linear calibration equation.

The ratio method's performance is characterized by the measurement of a subsequent sample and comparing the measured ratios to their respective calibration equations. The results will be evaluated based on the percent relative difference, $\%Diff. = \frac{Measured-Expected}{Expected} * 100\%$, as well as the average relative standard deviations for each parameter set.

The sample used to characterized the method was acquired six months after the initial data set and had a ^{235}U enrichment of 2.80%. A new 12-hour background was acquired in the same laboratory as prior samples under the same conditions. The sample was measured for four hours at a source-detector distance of 1.25 cm. A photo of the setup is shown in Fig. 15. Notably, this setup looks slightly different than the original setup shown in Fig.6. An array of thin lead sheets were added above the detector along with an additional Al filter to cut down the large background contribution from sources stored in the cabinets above.

Lastly, in order to provide a performance metric that is readily comparable to what is produced via the COMPUCEA system, a separate analysis

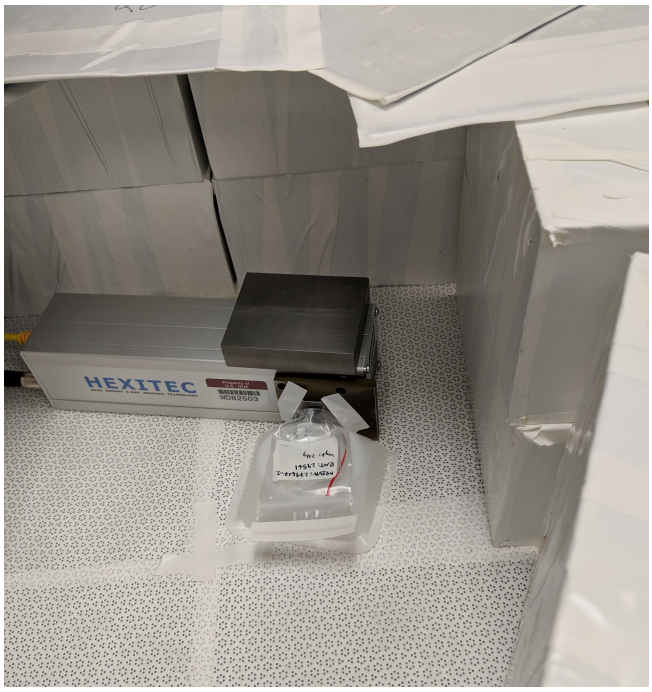

Figure 15: Photo of the experimental setup used for the supplemental measurement of the 2.80% sample.

was conducted in which some data points are intentionally excluded from the calibration equations. To this end, the optimum parameter set (Sec. 3.3.2) and only the 0.72%, 3.2% and 4.7% enriched uranium samples were used to create the 94/92 and 98/92 calibration equations. The four leftover uranium samples with ^{235}U enrichment 2.67%, 2.80%, 3.89% and 4.43% were analyzed using the new 3-point calibration equations. The two metrics used were the average bias percentage and the %RSD of the four bias percentages.

2.3.3 GEM Method

NaIGEM was originally released in 2001 as a ^{235}U enrichment analysis technique, specifically for NaI detectors [10, 11]. The method is reliant on accu-

rately measuring the prominent 186 keV peak from ^{235}U. In theory, as the enrichment increases, the 186 keV peak area should increase linearly. The analysis performs a peak fit with a background continuum subtraction. In order to produce reliable results, the NaIGEM software requires a calibration sample with known enrichment and any container properties that can be provided. The NaIGEM software was later adapted to be able to analyze spectra from detectors other than just NaI such as, $LaBr_3$ and CZT detectors of varying crystal dimensions. The adapted code is further referred to as GEM.

To calculate the enrichment of an unknown sample, one must first calibrate the software. To calibrate the software, a uranium spectrum with known enrichment and measurement conditions is loaded. Prior to loading the spectrum, it must first be converted such that it has exactly 4096 bins, else GEM will be unable to analyze.

The user is able to setup a custom configuration of different detector types/dimensions. A custom CdTe option was created for the HEXITEC detector. The GEM software does not currently have a CdTe crystal to choose from the "Detector type", therefore the CZT crystal option was chosen as they both exhibit low-energy hole-tailing and relatively similar energy resolutions. The crystal dimensions 1 mm length x 20 mm diameter. The collimator dimensions are 10 mm length x 10 mm diameter. Lastly, the peak model used is "Tailed Gaussian 1" which will include the hole-tailing feature in the peak fitting algorithm. With the correct detector properties

and source information, GEM is now able to calibrate based on the input sample spectrum.

The 4.7% ^{235}U sample was used for calibration as it has the most counts in the 186 keV peak. The spectrum fitting graph from the calibration sample is shown in Fig. 16.

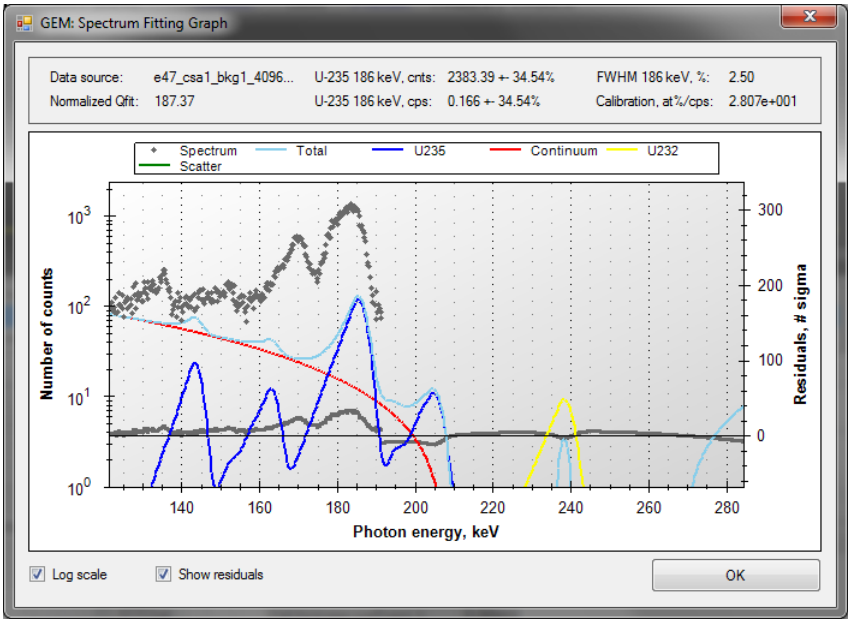

Figure 16: Shown is the fitting graph from GEM for the calibration sample of 4.7% ^{235}U, processed using the CSA algorithm.

The normalized Qfit from Fig. 16 is 187.37, which is a poor fit as is visually apparent. Each of the six uranium samples were ran through the calibration process to determine if a better normalized Qfit could be obtained. However, none of the six uranium samples were able to correctly fit the 186 keV peak. For this reason, future samples that were analyzed using this poor calibration equation yielded erroneous ^{235}U enrichment results e.g. values of

"infinity". These preliminary results illuminated the necessity for a proper CdTe crystal input, rather than CZT. An example of what a high-quality fit in the calibration step looks like, a HEU spectrum taken with a CZT detector is shown in Fig. 17.

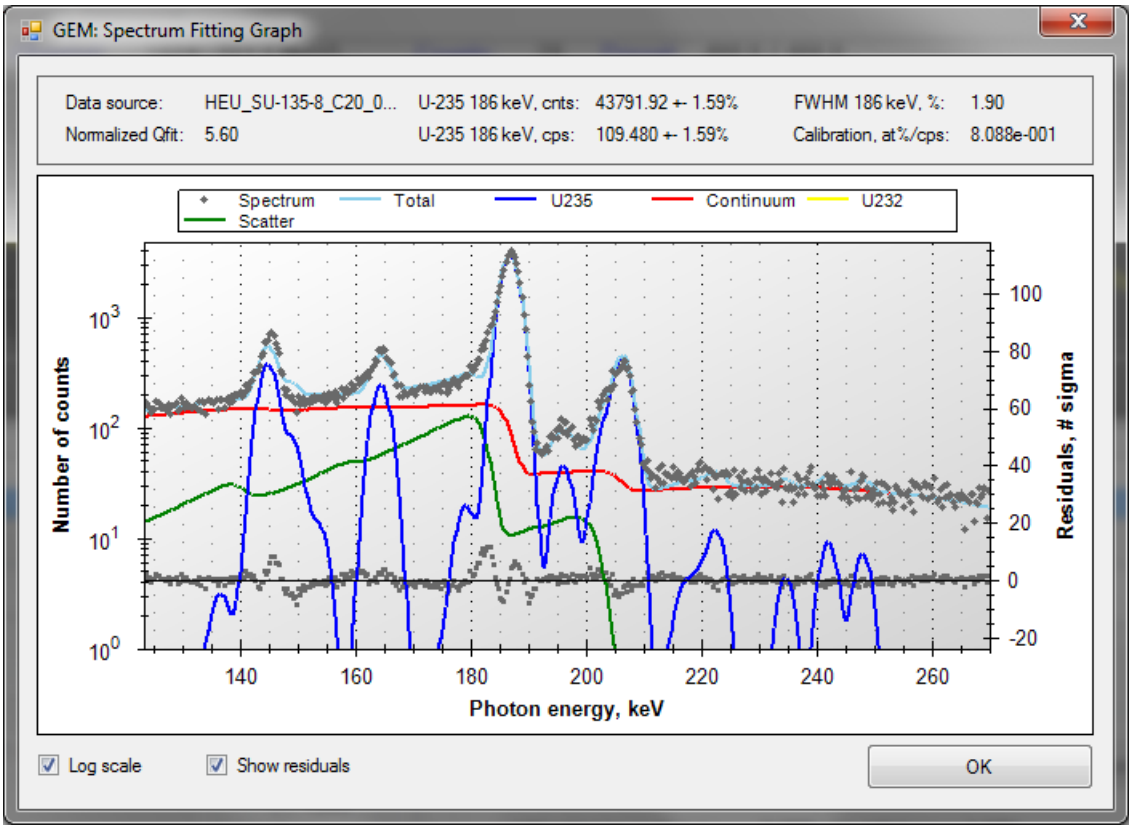

Figure 17: Plot of the fit components from GEM's analysis along with the residuals from the fit.

2.4 Modeling

MCNP6.2 is used to model the HEXITEC data acquisition system. LANL recently released MCNP6.2 which is described as an integration of MCNP5 and

MCNPX. It introduced new tools, bug fixes, and new features among other changes [28]. Included in these new tools is the MCNP Intrinsic Source Constructor (MISC) which is a library for generating intrinsic radiation sources for inputs into MCNP. Specifically, this new tool is used to generate the source definition (SDEF) for the MCNP input file used to model each of the measured enriched uranium pellets.

The MCNP model includes the CdTe detector crystal, the tungsten collimator, the enriched uranium pellet source, and lastly the lead shielding that surrounds the system. The input file defines these objects as well as the source information and is shown in Appendix A. Note, Appendix A does not show the source sampling information as the number of energies to sample that have nonzero probabilities spans 900 lines. Each simulation used a F8 tally with the mode set to photons only. The example input file used a 4.7% enriched uranium pellet sample with the same geometry as the experimental setup shown in Fig. 6.

Three different samples were modeled for comparison with enrichments 2.67, 3.9 and 4.7% ^{235}U. A total of 5×10^9 particles were simulated for each enrichment, requiring approximately 500 minutes to simulate using the Rogue cluster at OSU School of Nuclear Science and Engineering resulting in the output spectra that are idealized delta peaks. To transform these peaks to realistic CdTe peaks, which include Gaussian broadening and low-energy hole-tailing mechanisms, a DRF was applied to each spectrum using FORTRAN. The DRF used was created by the SpecX system's modeler, which

has undergone development for two years. The DRF captures unique properties about the detector such as the pixelation and the charge-sharing effects. The model was then evaluated based on visual inspection as well as the relative error associated with the important peaks for analysis e.g. 92.4, 92.8, 94.6, and 98.4 keV.

With a validated model, one can generate simulated enrichment spectra beyond the scope of what is readily available for measurement. This is one way to test each algorithm's ability to accurately analyze various enrichments e.g. high-enriched uranium (HEU). The simulated ^{235}U enrichments created in MCNP6.2 were 2.6725%, 4.7%, 6.0%, 20% and 60%. Again, these simulations result in ideal delta peaks and are passed through the DRF in FORTRAN to simulate true CdTe peaks. The output spectra is then analyzed using both the FRAM method and the ratio method to test their performance. In FRAM and the ratio method, parameter set 4 was used for reasons discussed later in Section 3.3.2.

3 Results

3.1 Detector Characterization

3.1.1 Energy Calibration

The energy calibration data was processed using the CSD and NFC algorithms. The energy response consistency can be seen in Fig. 18 and Table 4.

Fig. 18 shows a subset of ten pixel spectra chosen randomly. The primary 59.5 keV photopeak location from ^{241}Am is consistent across these pixels. Though there are minor differences observed in the shapes of the photopeaks, it is evident that the energy calibration is performing nominally. Note, the pixel spectra are vertically shifted. Relating to the consistency of the energy calibration for all detector pixels, Table 4 shows the mean and standard deviation of the photopeak locations after calibration. Each mean is compared to its known γ energy and the percent deviation is calculated by:

$$D_E = \left| \frac{(E_{known} - E_{measured})}{E_{known}} \right| * 100\% \tag{8}$$

The mean peak location error of $< 0.5\%$ for all four peaks is suitable for the algorithm. Greater than 99% of the pixels have photopeak locations within 3σ of the mean at all measured energies. However, this analysis includes 17 pixels with photopeak locations at 0 keV. These pixels are a combination of dead pixels due to poor bump-bonding between the ASIC and CdTe, as well as pixels that have their responses intentionally zeroed. These pixels are zeroed because they exhibit gain issues likely due to insufficient contact between the ASIC and CdTe, which results in a severe drop-off in efficiency at energies of interest.

A typical FWHM value for one of the pixels at 60 keV is approximately 0.80 keV, while the pixel-summed spectrum has a FWHM value of 0.86 keV. This slight increase in FWHM when combining all 6400 pixel re-

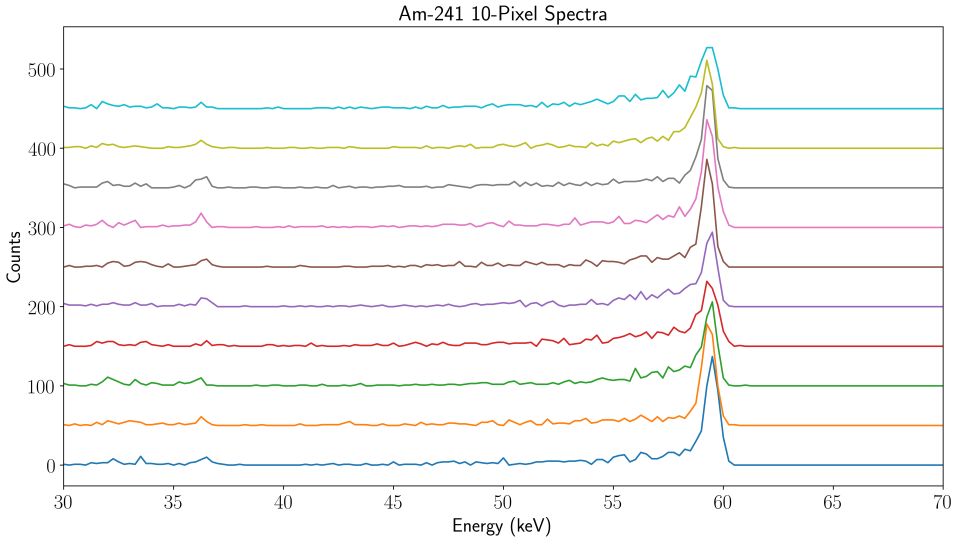

Figure 18: Spectra from ten randomly-selected pixels processed using the automated, custom pixel-by-pixel quadratic energy calibration. The source was ^{241}Am (0.498 mCi) and was measured for 10 minutes at a 10 cm stand-off distance.

Table 4: Shown are the quadratic energy calibration results. Included are the mean and standard deviation of the post- calibration photopeak locations, in keV, calculated for all 6400 pixels. Additionally, the deviation of each mean photopeak location from the known value is shown using Eq 8.

Known peak energy (keV)	$\mu_{Measured}$ (keV)	$\sigma_{Measured}$ (keV)	D_E (%)
30.97	30.98	0.12	0.03
59.54	59.26	0.89	0.47
81.00	81.05	0.09	0.06
122.06	121.80	0.15	0.21

sponses is an indication of a good pixel-by-pixel energy calibration.

3.1.2 Charge Sharing

Charge sharing effects can be significant in the HEXITEC V2 detector, as mentioned. Fig. 19 exhibits a direct comparison between the two charge-sharing algorithms, CSA and CSD, as well as the raw, unprocessed data.

Both methods are used in combination with NFC. The CSA approach contains more photopeak counts as expected, though the lower-energy tail is enhanced, broadening the photopeak width or FWHM. With the intention of measuring ^{235}U enrichment, energy resolution and detection efficiency both play key roles. Using the CSD approach may lead to fewer spectral artifacts, however the reduced number of photopeak counts could result in a underestimation of the enrichment.

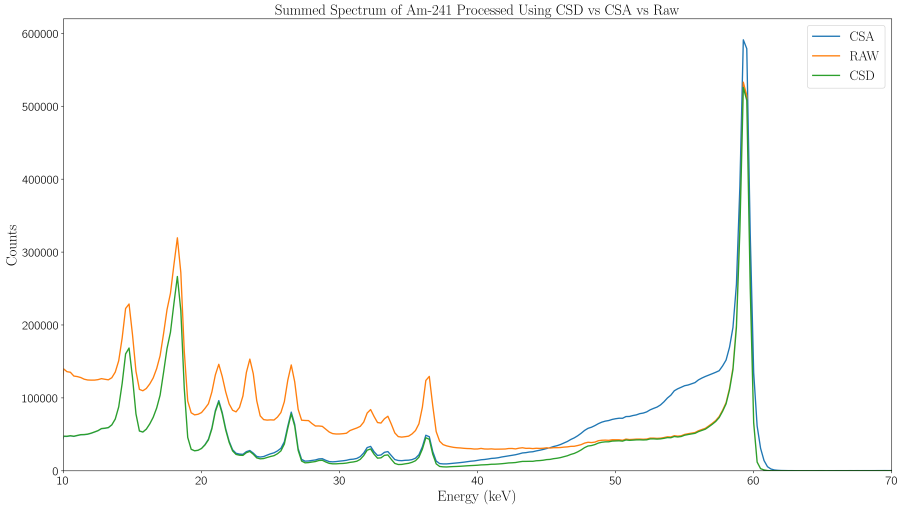

Figure 19: ^{241}Am (0.498 mCi) measured for 10 minutes at 10 cm standoff summed over all pixels. Data was processed using either the CSD (blue) or CSA (green) method. The raw spectrum (orange) is provided for comparison.

Despite being high-activity sources (0.498, 0.068, and 0.85 mCi), the ^{241}Am, ^{57}Co and ^{133}Ba sources only yield approximately 8, 3, and 28 counts/frame respectively, corresponding to 6.4e4, 2.4e4, 2.2e5 counts/s on the detector face. In typical X-ray operation for the SpecX system this is elevated to $>$ 700 counts/frame, corresponding to 5.8e6 counts/s, even with

shielding and a 2m stand-off. Further, the 4.4% enriched uranium data, processed using the CSA and NFC methods yield only 0.24 counts/frame, corresponding to 48 counts/s. However, it has been observed that the count rate values will vary between uranium samples. The number of removed events is a function of incident energy, interaction depth and the number of events per frame. It is critical for these charge-shared events be corrected via the CSD or CSA method. Without correction, these charge-shared events will add to the enrichment uncertainty. The results from the event removal analysis for the different sources are compiled in Table 5.

Table 5: Charge-sharing correction results from a flat-field measurement using ^{241}Am, ^{57}Co, ^{133}Ba and a commercial Comet 160 kVp X-ray source. Additionally, a 4.4% enriched uranium dataset is provided for comparison.

Source	Total Events	CSD removed	NFC removed	$\frac{Removed}{(Total+Removed)}$
^{241}Am	8,865,886	5,819,982	368,423	0.411
^{133}Ba	40,799,206	28,783,481	1,834,877	0.429
^{57}Co	1,043,688	1,060,345	58,366	0.517
U	1,572,026	880,732	1,395	0.561
X-ray	511,650,532	967,784,777	91,565,154	0.674

3.1.3 Detector Stability

It is important in a detection system that the data remains stable throughout the entirety of the acquisition. The HEXITEC detector is capable of recording the crystal temperature while the bias voltage is applied. To this point, the crystal temperature remained stable over the testing period . There were no notable impacts observed on the spectral performance due to tempera-

ture effects, specifically the photopeak counts as shown in Fig. 20, or the photopeak location. A pixel-by-pixel stability analysis was not conducted due to the low number of counts in each pixel. Much longer acquisitions would be needed to precisely study individual pixel stability. However, the summed-pixel response of the system is a strong indicator of overall system stability. The mean and standard deviation of the summed photopeak counts over the 13 ten-minute acquisitions is: $\mu = (4.0674 \pm 0.0006) \times 10^6$ counts. Table 6 tabulates the predicted statistical standard deviation (σ_{Stat}), assuming the observed photopeak counts are Poisson distributed, in comparison to the measured standard deviation ($\sigma_{measured}$), for the four photopeaks. These values were calculated for 13 ten-minute acquisitions for ^{241}Am (59.5 keV), 7 acquisitions for ^{133}Ba (31 and 81 keV) and 8 acquisitions for ^{57}Co (122 keV).

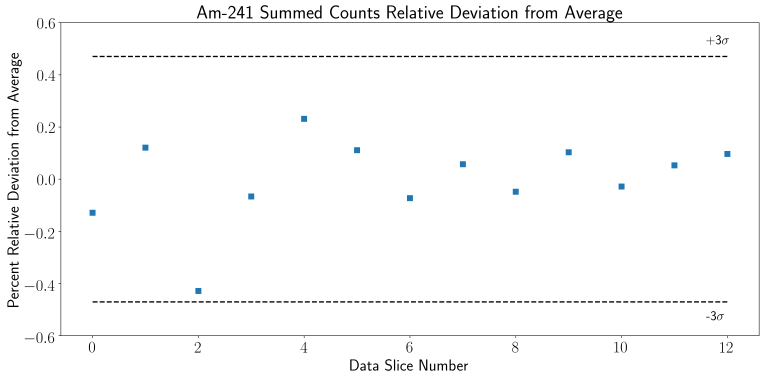

Figure 20: The percent relative deviation from the mean photopeak counts with 3σ lines shown. Calculations based on ^{241}Am (0.498 mCi) source measured in consecutive 10-minute segments at 10 cm standoff summed over all pixels..

Table 6: The total and statistical errors in the net photopeak counts were computed for acquisitions under identical conditions. In all cases the predicted statistical uncertainty is small compared to the measured uncertainty.

Energy (keV)	$\sigma_{measured}$ (%)	σ_{Stat} (%)
30.97	0.750	0.026
59.54	0.237	0.048
81.00	1.072	0.048
122.06	0.828	0.152

3.2 Sample Measurement

The eight measured UO_2 pellets were processed for enrichment analysis using a number of different parameter sets (Table 2). Including CSA vs CSD, charge sharing grid 3x3 vs 5x5, bin width of 50 eV vs 250 eV, background 1 vs background 2 subtraction, and ROI (region of interest) vs non-ROI analysis. The default parameters that were selected, unless specified otherwise, are CSA, 3x3, 250 eV, background2, and ROI. The spectrum and image of the 3.9% enriched pellet sample processed using these default parameters are shown in Figs. 21 - 22.

Fig. 21 reveals interesting features, note the unknown peak at 176 keV. First, there is a noticeable low-energy peak at the energy cutoff threshold of 5 keV due to detector noise and low-energy uranium peaks. Second, the most prominent peaks in the spectrum are the 90-100 keV peaks of interest. Lastly, the 186 keV peak from ^{235}U has a substantial FWHM (8 keV). This is likely due to the fact that 186 keV is near the end of the detector's range and there are two uranium peaks at 201 and 202 keV that can lose

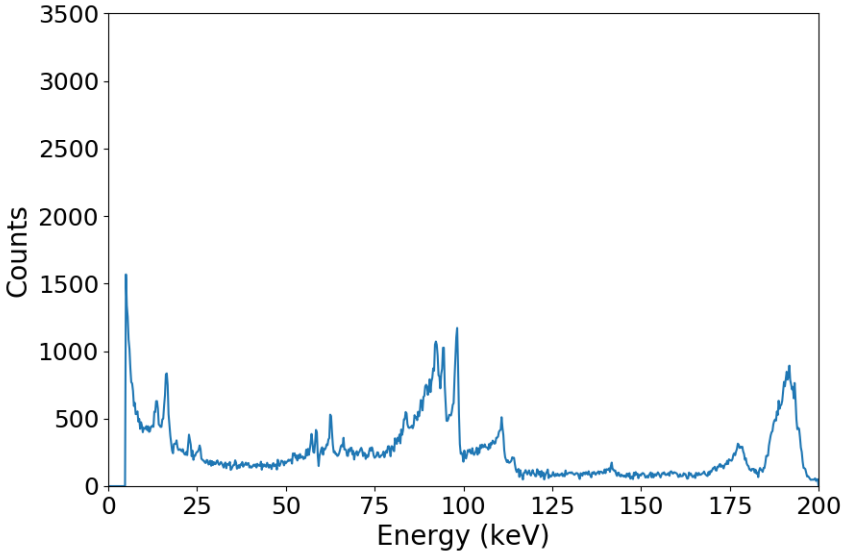

Figure 21: Spectrum of the 3.9% enriched uranium pellet processed using all default parameters.

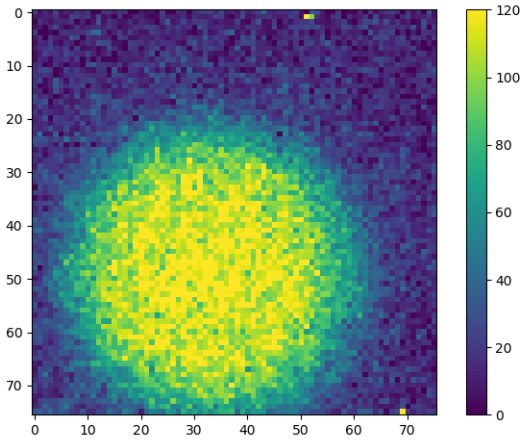

Figure 22: Image of the 3.9% enriched uranium pellet processed using all default parameters.

energy to blur the 186 keV peak. Also, if the pixel-by-pixel quadratic energy calibration is imperfect then the end of the energy range can experience peak broadening. This broadening is especially problematic for enrichment codes that are heavily dependent on the 186 keV peak (e.g. MGAU, GEM, and

FRAM). However, in some cases the 186 keV peak can be excluded from the analysis to help with this issue.

Only six out of the eight pellet samples were used in the actual analysis. The pellet slices were difficult to maintain ideal geometry while double-bagged i.e. the flat face of the pellet parallel to the detector face and concentric with the collimator hole. The ROI-summed spectra (processed using default parameters) from the six samples can be seen in Fig. 23.

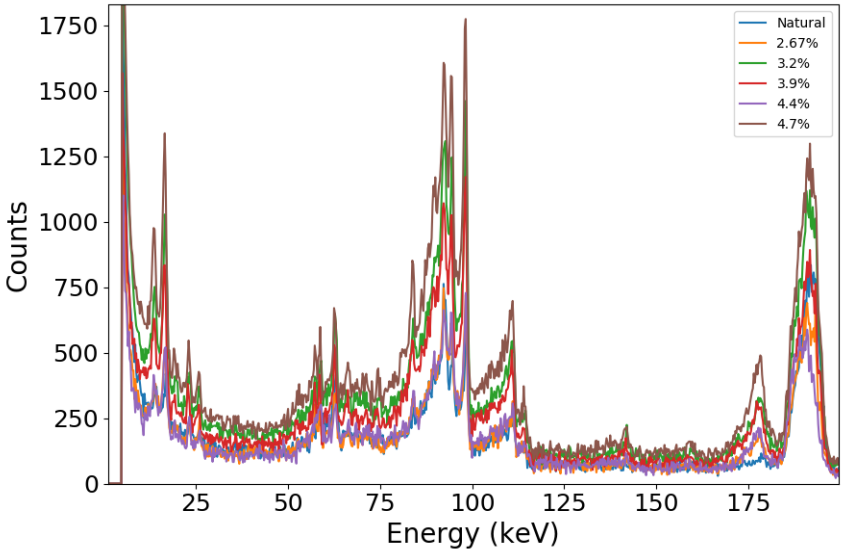

Figure 23: Shown are the six ROI-summed spectra from the measured pellet samples, processed using default parameters.

To observe how each parameter will affect the summed spectral response, Figs. 24-28 illustrate changing one parameter at a time from the default parameter set. Again, the 3.9% enriched pellet sample was chosen to compare.

Fig. 24 displays a lower background in the CSD spectrum, however

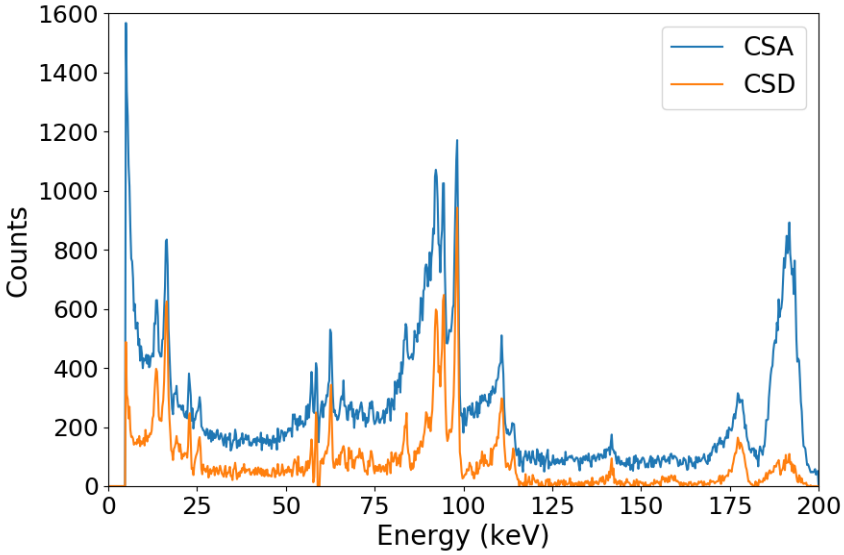

Figure 24: Two spectra from the 3.9% enriched pellet processed using CSA vs CSD, all other parameters were left default.

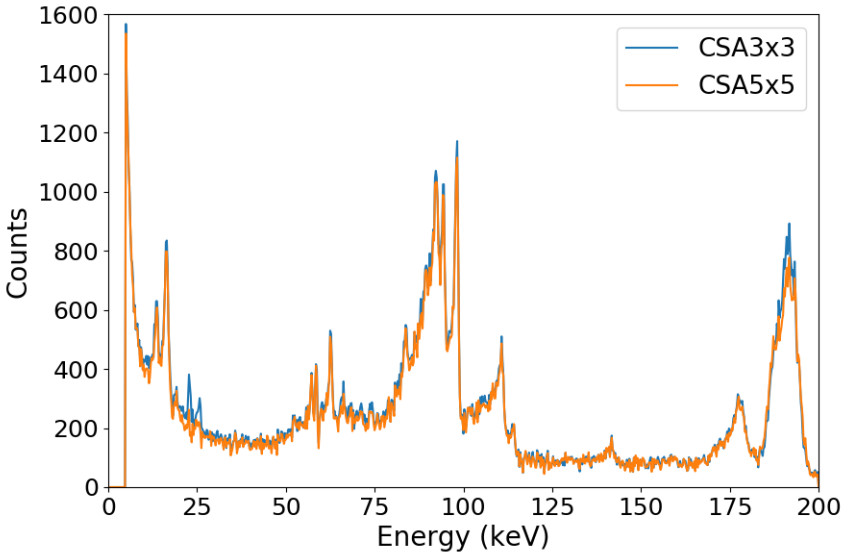

Figure 25: Two spectra from the 3.9% enriched pellet processed using CSA3x3 vs CSA5x5, all other parameters were left default.

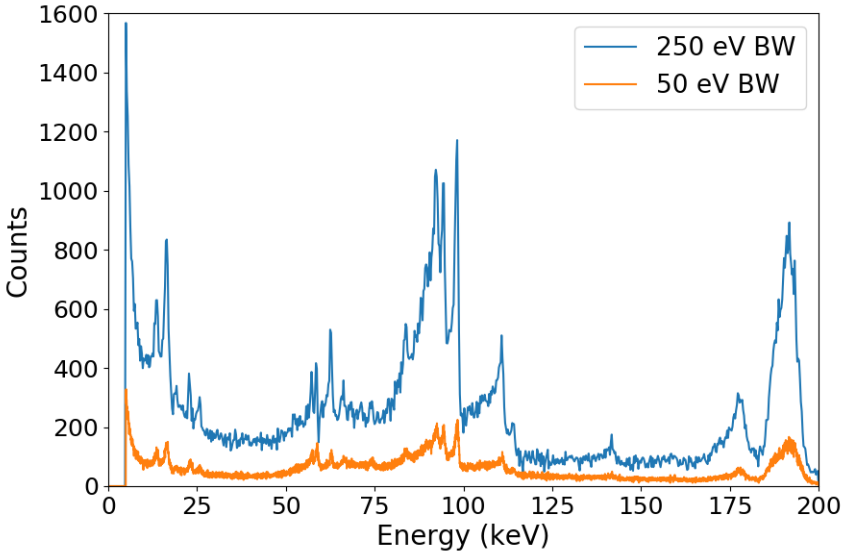

Figure 26: Two spectra from the 3.9% enriched pellet processed using CSA with 250 eV bin width vs CSA with 50 eV bin width, all other parameters were left default.

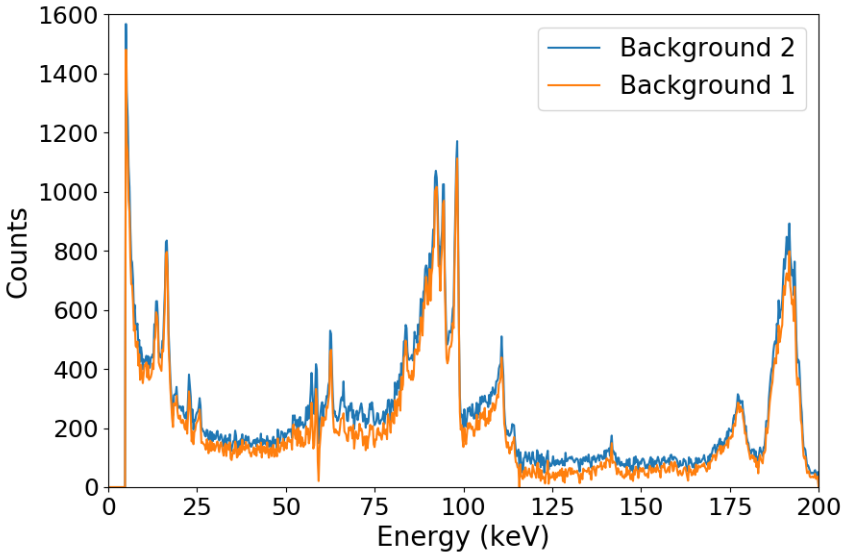

Figure 27: Two spectra from the 3.9% enriched pellet processed using CSA with background 1 subtracted vs CSA with background 2 subtracted, all other parameters were left default.

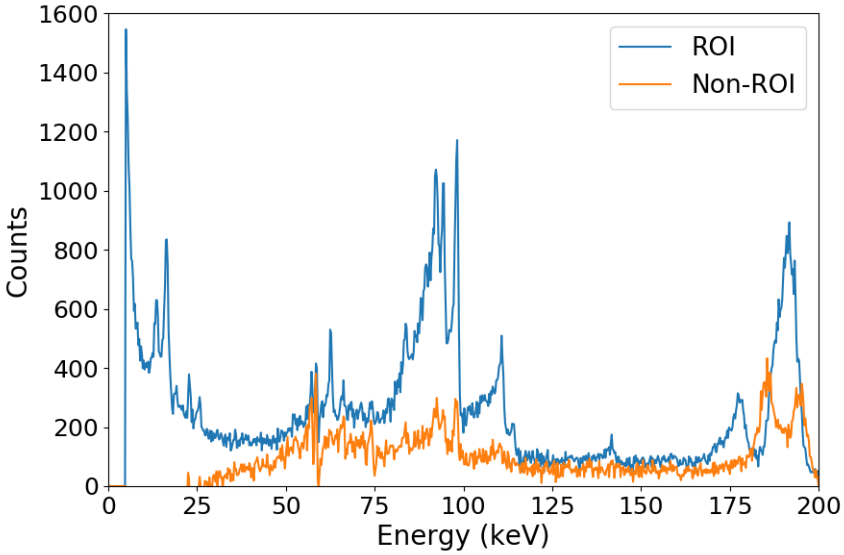

Figure 28: Two spectra from the 3.9% enriched pellet where only the pixels labeled with a red dot in Fig. 29 are summed for the ROI spectrum, all other pixels are summed to form the Non-ROI spectrum. Other parameters were left default.

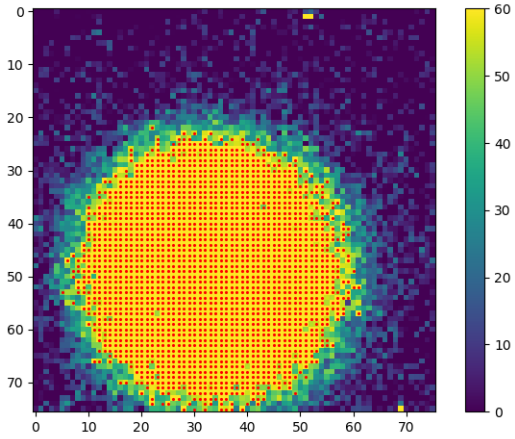

Figure 29: The pixel-summed image of the 3.9% enriched pellet with ROI pixels specified with red dots.

there are far fewer counts in each photopeak of interest. In specific, the 186 keV peak is almost non-existent in the CSD spectrum, but there is a prominent, yet blurred, peak in the CSA spectrum. This is due to the charge-

sharing having a strong energy dependence, i.e. a larger energy photon (186 keV) will generate a charge cloud that spans more pixels, which are then removed via the CSD mechanism.

It appears (Fig. 25) that there is almost no difference observed between the CSA 3x3 processing as compared to the CSA 5x5. The only noticeable shift is a slight decrease in net counts in the 186 keV peak using the CSA 5x5 approach.

In Fig. 26 the most notable distinction is the large difference in net counts in each bin when varying the bin width from 250 eV to 50 eV. However, the net area of counts for each peak is the same. When scaled, the 250 eV bin width spectrum will appear less noisy, which is the reason it is chosen as a default parameter.

Minor differences are observed between the two background subtraction methods, as seen in Fig. 27. Slightly more counts in the 90-100 keV photopeaks are observed when subtracting background 2, with a minor increase in backgrounds counts as well.

Lastly, in Fig. 28 the pixels selected for the direct-beam ROI are summed and plotted for comparison against the summed pixels that were not selected. Further, the non-ROI spectrum shows two peaks in the 180-200 keV region that would contribute to the 186 keV peak's FWHM if included in the analysis. The selected pixels are shown as red dots in Fig. 29. It is noted that the non-ROI spectrum is mostly noise.

3.3 Enrichment Analysis Algorithms

3.3.1 FRAM Method

The FRAM uranium enrichment analysis algorithm version 5.2 comes with default CdTe parameters. The parameter file was altered slightly to remove the peaks > 200 keV from the analysis, as this is not within the energy range of the HEXITEC. A variety of processing techniques were explored to determine which combination of processing tools would aid FRAM in correctly identifying the enrichment. The parameters that were considered are as follows: bin width, charge-sharing correction grid, CSA vs CSD, subtraction of background 1 or background 2 and lastly using an ROI vs non-ROI approach.

Table 7: Results from FRAM using parameters 250 eV width, 3x3 charge sharing grid, CSA, background 2, and no ROI.

Declared (%)	FRAM Calc. (%)	Measured-Declared	Sigma	%Diff.	%RSD
0.72	5.253	4.5332	10.499	86.29	> 100
2.6725	2.846	0.1735	2.846	6.10	100
3.2	3.666	0.466	0.710	12.71	19.36
3.8862	6.462	2.576	1.059	39.86	16.38
4.4308	2.914	-1.517	0.4913	-52.06	16.86
4.7	7.103	2.403	0.980	33.83	13.80

The results (Table 7) do not indicate strong agreement between the calculated FRAM enrichments and their reference values. The absolute average difference between measured and declared is 1.94% ^{235}U; in a practical sense, an error of 2% would be unacceptable. Further, the sigma values are observed to generally decrease with an increase in enrichment within this

range. This is likely derived from the higher enriched samples having more counts, allowing the FRAM algorithm to calculate a smaller sigma. Lastly, as seen in Table 7, FRAM over-estimates the enrichment in all cases except for the 4.43% enriched sample.

Table 8: Results from FRAM using parameters 50 eV width, 3x3 charge sharing grid, CSD, background 1, and no ROI.

Declared (%)	FRAM Calc. (%)	Measured-Declared	Sigma	%Diff.	%RSD
0.72	2.093	1.373	0.561	65.59	26.79
2.6725	3.281	0.608	0.808	18.54	24.63
3.2	4.129	0.929	0.916	22.49	22.18
3.8862	4.59	0.704	0.864	15.33	18.82
4.4308	4.069	-0.362	0.799	-8.91	19.64
4.7	6.881	2.181	0.737	31.69	10.72

Results from changing the bin width to 50 eV, using CSD and background 1 (Table 8) also do not show strong agreement between the calculated FRAM enrichments and their reference values. The absolute average difference between the measured and declared values is 1.03% ^{235}U. This is a decrease of roughly one half the deviation observed in Table 7. There were three parameters changed between these two sets of results, the bin width was reduced $250eV \rightarrow 50eV$, CSA $\rightarrow$ CSD, and lastly background 1 was subtracted instead of background 2. Most notably, the sigma values drastically decreased from between the parameter sets. This is likely due to the CSA approach having more uncertainty in the summing mechanism as mentioned in Section 2.1.2.

Table 9: Results from FRAM using parameters 50 eV width, 3x3 charge sharing grid, CSA, no background subtracted, and no ROI.

Declared (%)	FRAM Calc. (%)	Measured-Declared	Sigma	%Diff.	%RSD
0.72	2.908	2.188	1.027	75.24	35.33
2.6725	3.369	0.697	0.877	20.68	26.02
3.2	5.535	2.335	1.839	42.18	33.22
3.8862	5.792	1.906	1.228	32.90	21.20
4.4308	4.150	-0.281	1.119	-6.78	26.97
4.7	7.720	3.020	3.933	39.12	50.95

The results from Table 9 show a greater deviation between measured and reference as compared to the first two parameter sets analyzed. The absolute average difference between measured and declared values is 2.19% ^{235}U. This increase from the last two datasets is likely due to the fact that no background was subtracted. Without background subtraction, a higher rate of noise was allowed into the spectrum, which is known to have counts in the 186 keV region that can lead to over-estimating the enrichment.

Table 10: Results from FRAM using parameters 250 eV width, 3x3 charge sharing grid, CSA, background 1, and ROI.

Declared (%)	FRAM Calc. (%)	Measured-Declared	Sigma	%Diff.	%RSD
0.72	0.647	-0.070	0.654	-10.84	100.69
2.6725	2.1675	-0.505	0.773	-23.30	35.67
3.2	3.532	0.332	0.593	9.40	16.78
3.8862	5.482	1.596	1.185	29.11	21.62
4.4308	3.014	-1.417	0.500	-46.99	16.58
4.7	6.097	1.397	0.978	22.91	16.04

The results from Table 10 are compelling. The sigma values are

all less than 1, except for the 3.9% sample. Further, the absolute average difference between measured and reference values is 0.89% ^{235}U which is the smallest deviation thus far.

Table 11: Results from FRAM using parameters 250 eV width, 3x3 charge sharing grid, CSA, background 2, and ROI.

Declared (%)	FRAM Calc. (%)	Measured-Declared	Sigma	%Diff.	%RSD
0.72	0.677	-0.043	0.751	-6.33	110.94
2.6725	2.697	0.025	1.143	0.91	42.36
3.2	3.263	0.063	0.563	1.93	17.24
3.8862	3.684	-0.203	0.484	-5.50	13.12
4.4308	3.131	-1.300	0.442	-41.54	14.13
4.7	6.116	1.416	0.979	23.15	16.01

Table 11 conveys strong correlation between the measured and reference values for samples 0.72% $\rightarrow$ 3.9%, for these samples the absolute average difference between measured and observed is 0.08% ^{235}U. For the full set of samples, this absolute average difference jumps to 0.45% ^{235}U which still shows greater agreement than Tables 7-10. Further, none of the sigma values appear erroneous, as only the 2.67% sample has a sigma value greater than 1, leading to manageable %RSD values in the range of 10-20%.

Table 12 does not suggest strong agreement between the measured and declared uranium enrichments. The absolute percent difference varies between 10-20% for the samples with larger than 0.72% enrichment. The 4.43% sample is underestimated by FRAM in every result, which indicates that there was likely an issue with data acquisition for this sample. Further,

Table 12: Results from FRAM using parameters 250 eV width, 3x3 charge sharing grid, CSD, background 1, and ROI.

Declared (%)	FRAM Calc. (%)	Measured-Declared	Sigma	%Diff.	%RSD
0.72	1.117	0.397	0.733	35.55	65.62
2.6725	2.364	-0.309	0.955	-13.07	40.40
3.2	3.863	0.663	0.700	17.16	18.11
3.8862	4.855	0.969	0.884	19.96	18.21
4.4308	3.864	-0.567	0.668	-14.67	17.29
4.7	5.189	0.489	0.549	9.43	10.59

using parameter set 6 also caused the 2.67% sample to be underestimated. Thus far, the only other parameter set that caused the 2.67% sample to be underestimated was parameter set 4. These two parameter sets are unique, as they are the using the CSA processing algorithm, a background 1 subtraction and an ROI approach.

Table 13: Results from FRAM using parameters 250 eV width, 3x3 charge sharing grid, CSD, background 2, and ROI.

Declared (%)	FRAM Calc. (%)	Measured-Declared	Sigma	%Diff.	%RSD
0.72	0.306	-0.414	0.255	-135.00	83.36
2.6725	1.734	-0.939	0.2754	-54.17	15.89
3.2	3.739	0.539	0.580	14.40	15.51
3.8862	5.106	1.220	0.740	23.89	14.50
4.4308	3.923	-0.508	0.663	-12.95	16.91
4.7	5.455	0.755	0.527	13.84	9.67

The findings from parameter set 7 are similar to those in parameter set 6. The main difference stems from the 0.72% sample now also being underestimated by FRAM. The common parameter setting across the three

parameter sets that underestimate the 2.67% sample is the ROI being utilized. Therefore, it can be asserted that using the ROI approach is observed to cause FRAM to estimate less ^{235}U.

The average difference between the measured and declared ^{235}U enrichment from implementing the seven parameter sets in FRAM are plotted in Fig. 30. The average absolute difference drops from 1-2% to 0.5-1% when the analysis begins using an ROI. The largest absolute deviation is seen in parameter set 3, where the background was not subtracted. Further, the smallest absolute deviation comes from the use of parameter set 5. The calculated enrichments for the 0.72%, 2.67% and 3.2% all deviate by less than 0.064% from their references using this parameter set, with an average absolute deviation of 0.044%. These values compare well to the results shown by Yucel (2008) and Brodsky (2008) [18,20]. However, the calculated enrichment values for the 4.43% and 4.7% do not match as well as the previous three calculated enrichments. These two samples did not match their reference values using any of the shown combination of parameters, this indicates there may have been an issue with the data collection. This could be due to unknown sources being moved near the detector during acquisition, as the samples were measured in a high gamma background laboratory. This could be verified by looking at the counts per second (cps) during the entirety of the acquisition.

The compilation of results from FRAM indicate that, even while using the best parameter settings, FRAM does not produce results that are

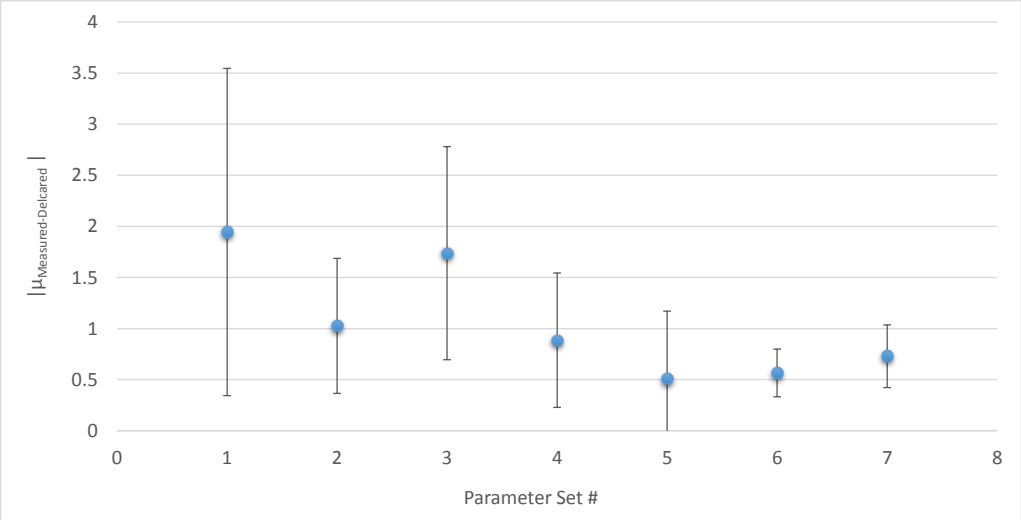

Figure 30: Depicts the average absolute difference between the measured and declared uranium enrichments for the seven parameter sets using FRAM.

comparable to COMPUCEA's %RSD values of 0.45% using the HEXITEC system. This is most likely due to the HEXITEC detector having a poor 186 keV peak response, which was included in the FRAM analysis.

3.3.2 Ratio Method

The ratio method relies upon accurate peak area estimation of the photopeaks in the 90-100 keV region of the uranium spectrum. To obtain an accurate peak area estimate the FRAM output was used. Similar to the FRAM method in section 3.1.1, the data was processed using the seven parameter sets in Table 2. Table 14 displays the peak areas along with the two ratio values at each enrichment measured for parameter set 1. Table 15 tabulates statistical standard deviations associated with the values in the previous table. Lastly, each figure plots the intensity ratios vs the certified enrichments

with the fitted linear equation and the R^2 goodness of fit coefficient.

Table 14: Peak area estimates from FRAM using parameter set 1 from Table 2.

Declared (%)	92* Peak	94.6 keV Peak	98.4 keV Peak	94/92 Ratio	98/92 Ratio
0.72	1864	452	2996	0.2425	1.6073
2.6725	3188	3013	2563	0.9451	0.8040
3.2	6790	7026	10616	1.0348	1.5635
3.8862	3801	4440	6527	1.1681	1.7172
4.4308	4102	5057	6899	1.2328	1.6819
4.7	6541	9167	13355	1.4015	2.0417

Table 15: Table containing the standard deviation for each of the three peaks used in the ratio method analysis as well as the standard deviations of the ratios themselves. Results refer to data processed using parameter set 1 from Table 2.

Declared (%)	σ_{92^*} (counts)	$\sigma_{94.6}$ (counts)	$\sigma_{98.4}$ (counts)	$\sigma_{94/92}$	$\sigma_{98/92}$
0.72	1094	452	641	0.0127	0.0474
2.6725	3188	3013	2563	0.0240	0.0213
3.2	658	511	480	0.0176	0.0243
3.8862	379	329	302	0.0258	0.0350
4.4308	484	376	347	0.0259	0.0332
4.7	551	461	425	0.0227	0.0308

The R^2 goodness of fit coefficient is 0.969 for the 94/92 line, while it is 0.176 for the 98/92 line. An R^2 value of 0.97 is acceptable and could be used to produce meaningful results as a calibration equation, however an R^2 value of 0.18 shows very little linearity. The poor fit from the 98/92 calibration line is predominantly due to the 0.72% as seen in Fig. 31. Further, the standard deviation for the 0.72% sample for the 98/92 ratio is the largest of all the measured samples at 0.0474.

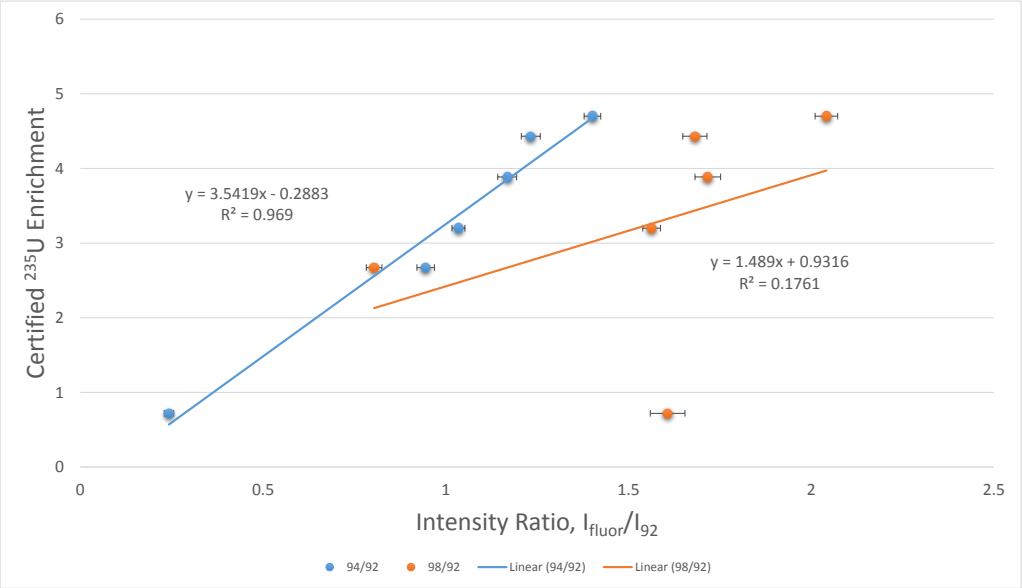

Figure 31: Intensity ratios 94.6 keV X-ray to 92* keV γ-ray and the 98.4 keV X-ray to 92* keV γ-ray plotted versus certified ^{235}U enrichment for parameter set 1. The linear fit to each set of data is shown with the associated fit equation and the R^2 coefficient.

Table 16: Peak area estimates from FRAM using parameter set 2 from Table 2.

Declared (%)	92* Peak	94.6 keV Peak	98.4 keV Peak	94/92 Ratio	98/92 Ratio
0.72	1612	780	1253	0.4839	0.7773
2.6725	1640	1504	2529	0.9171	1.5421
3.2	2518	2162	3616	0.8586	1.4361
3.8862	1794	1657	2581	0.9236	1.4387
4.4308	1742	1624	2451	0.9323	1.4070
4.7	3996	5394	8341	1.3499	2.0873

The results in Tables 14-15 and Fig. 32 using parameter set 2 show worse performance than parameter set 1. The R^2 coefficients for the 94/92 and 98/92 calibration equations are 0.760 and 0.685 respectively. In this case, neither calibration equation could be used to produce accurate results.

Table 17: Table containing the standard deviation for each of the three peaks used in the ratio method analysis as well as the standard deviations of the ratios themselves. Results refer to data processed using parameter set 2 from Table 2.

Declared (%)	σ_{92^*} (counts)	$\sigma_{94.6}$ (counts)	$\sigma_{98.4}$ (counts)	$\sigma_{94/92}$	$\sigma_{98/92}$
0.72	119	90	94	0.0211	0.0293
2.6725	129	107	112	0.0327	0.0489
3.2	167	152	176	0.0252	0.0373
3.8862	149	139	151	0.0315	0.0442
4.4308	148	112	136	0.0322	0.0441
4.7	210	197	207	0.0282	0.0402

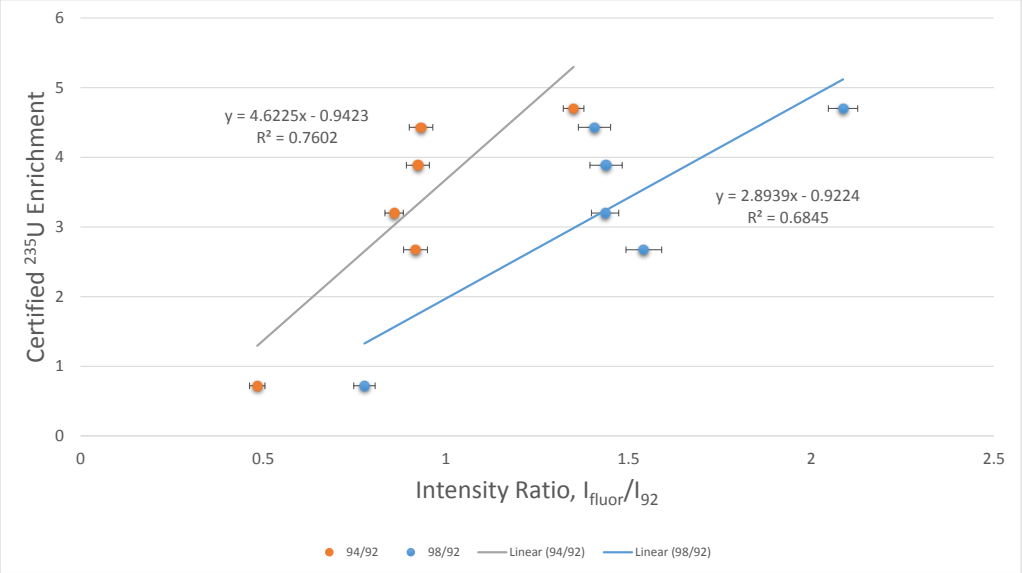

Figure 32: Intensity ratios 94.6 keV X-ray to 92* keV γ-ray and the 98.4 keV X-ray to 92* keV γ-ray plotted versus certified ^{235}U enrichment for parameter set 2. The linear fit to each set of data is shown with the associated fit equation and the R^2 coefficient.

The standard deviations associated with the ratios in Table 17 are larger on all accounts compared to those in Table 15, excluding the erroneous 0.72% sample discussed previously. Considering the number of data points that do not fall on the fitted line, this parameter set should not be used for

quantitative analysis using the ratio method.

Table 18: Peak area estimates from FRAM using parameter set 3 from Table 2 .

Declared (%)	92* Peak	94.6 keV Peak	98.4 keV Peak	94/92 Ratio	98/92 Ratio
0.72	2240	1024	1462	0.4571	0.6527
2.6725	2074	1971	2778	0.9503	1.3394
3.2	3444	2726	3937	0.7915	1.1432
3.8862	3200	3417	4825	1.0678	1.5078
4.4308	2301	2026	2688	0.8805	1.1682
4.7	5197	6389	8783	1.2294	1.6900

Table 19: Table containing the standard deviation for each of the three peaks used in the ratio method analysis as well as the standard deviations of the ratios themselves. Results refer to data processed using parameter set 3 from Table 2.

Declared (%)	σ_{92^*} (counts)	$\sigma_{94.6}$ (counts)	$\sigma_{98.4}$ (counts)	$\sigma_{94/92}$	$\sigma_{98/92}$
0.72	151	123	132	0.0172	0.0219
2.6725	181	140	146	0.0293	0.0378
3.2	273	225	235	0.0203	0.0267
3.8862	214	186	191	0.0262	0.0343
4.4308	206	177	169	0.0267	0.0331
4.7	333	302	298	0.0229	0.0295

The results using parameter set 3 are similar to those produced using parameter set 2. Specifically, the 4.43% sample appears to be an outlier yet again. The R^2 coefficients for the 94/92 and 98/92 calibration equations are 0.751 and 0.703 respectively. As with the coefficients from parameter set 2, these R^2 values are not good enough to produce repeatable results. The poor fits can be seen in Fig. 33. This is likely due to the fact that no background was subtracted for the analysis which added noise to each peak.

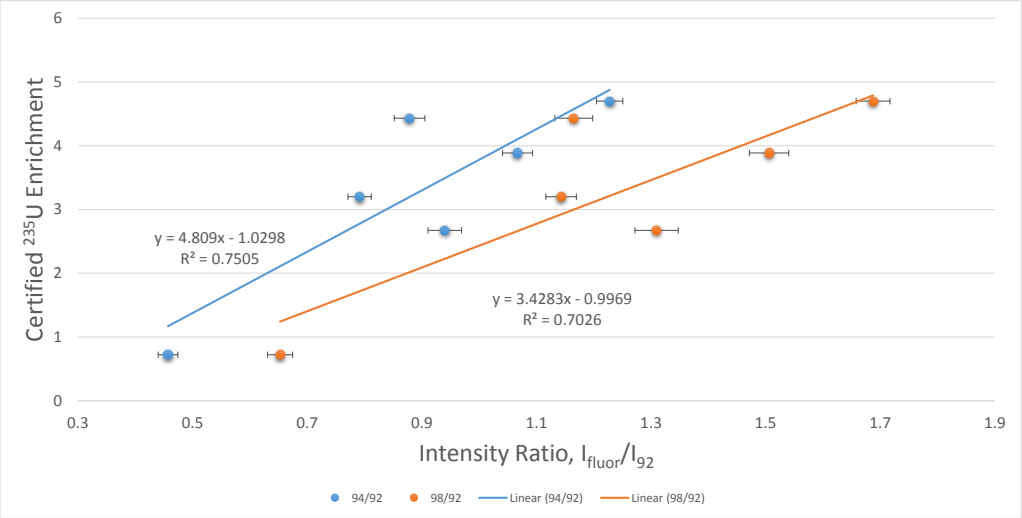

Figure 33: Intensity ratios 94.6 keV X-ray to 92* keV γ-ray and the 98.4 keV X-ray to 92* keV γ-ray plotted versus certified ^{235}U enrichment for parameter set 3. The linear fit to each set of data is shown with the associated fit equation and the R^2 coefficient.

Table 20: Peak area estimates from FRAM using parameter set 4 from Table 2 .

Declared (%)	92* Peak	94.6 keV Peak	98.4 keV Peak	94/92 Ratio	98/92 Ratio
0.72	3767	2025	3275	0.5376	0.8694
2.6725	1745	1472	2262	0.8436	1.2963
3.2	6612	6588	9934	0.9964	1.5024
3.8862	3453	3777	5574	1.0938	1.6143
4.4308	3431	4161	5813	1.2128	1.6943
4.7	6203	8469	11752	1.3653	1.8946

Beginning with parameter set 4, the ROI approach was implemented rather than using all pixels for analysis. Fig. 34 shows an increase in performance. Notably, the R^2 coefficients for the 94/92 and 98/92 calibration equations are 0.975 and 0.981 respectively. These values compare well with the coefficients found using a HPGe detector [18]. Further, the standard devi-

Table 21: Table containing the standard deviation for each of the three peaks used in the ratio method analysis as well as the standard deviations of the ratios themselves. Results refer to data processed using parameter set 4 from Table 2.

Declared (%)	σ_{92^*} (counts)	$\sigma_{94.6}$ (counts)	$\sigma_{98.4}$ (counts)	$\sigma_{94/92}$	$\sigma_{98/92}$
0.72	394	299	260	0.0148	0.0208
2.6725	248	197	183	0.0299	0.0413
3.2	530	411	378	0.0173	0.0238
3.8862	430	354	309	0.0258	0.0350
4.4308	390	322	283	0.0280	0.0365
4.7	634	523	463	0.0228	0.0297

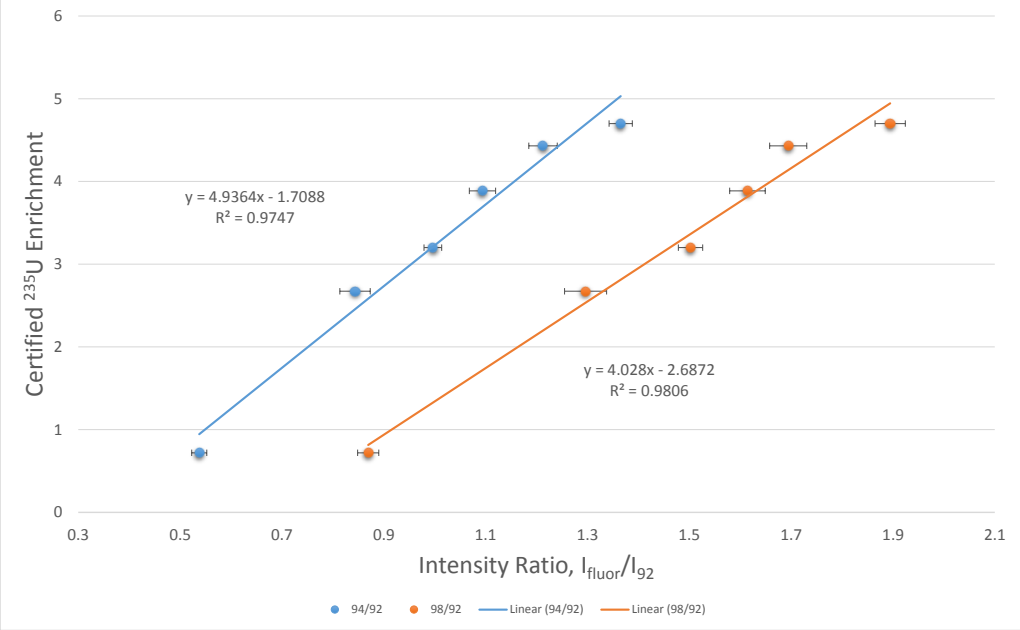

Figure 34: Intensity ratios 94.6 keV X-ray to 92* keV γ-ray and the 98.4 keV X-ray to 92* keV γ-ray plotted versus certified ^{235}U enrichment for parameter set 4. The linear fit to each set of data is shown with the associated fit equation and the R^2 coefficient.

ations for the ratio values shown in Table 21 have all decreased from previous parameter sets. In the case of parameter set 4, the R^2 coefficients suggest a strong linear correlation which should allow for enrichment determination

for subsequently measured samples.

Table 22: Peak area estimates from FRAM using parameter set 5 from Table 2 .

Declared (%)	92* Peak	94.6 keV Peak	98.4 keV Peak	94/92 Ratio	98/92 Ratio
0.72	3711	2016	3242	0.5433	0.8736
2.6725	2414	2176	3088	0.9014	1.2792
3.2	6825	6876	10115	1.0075	1.4821
3.8862	3706	4336	6272	1.1700	1.6924
4.4308	3758	4577	6341	1.2179	1.6873
4.7	6169	8495	11797	1.3771	1.9123

Table 23: Table containing the standard deviation for each of the three peaks used in the ratio method analysis as well as the standard deviations of the ratios themselves. Results refer to data processed using parameter set 5 from Table 2.

Declared (%)	σ_{92^*} (counts)	$\sigma_{94.6}$ (counts)	$\sigma_{98.4}$ (counts)	$\sigma_{94/92}$	$\sigma_{98/92}$
0.72	407	306	266	0.0150	0.0210
2.6725	322	255	224	0.0266	0.0348
3.2	546	424	388	0.0172	0.0232
3.8862	366	308	283	0.0262	0.0351
4.4308	401	331	294	0.0268	0.0347
4.7	629	518	461	0.0230	0.0300

The ratio method appear to be slightly better when using parameter set 5 over parameter set 4 in terms of R^2 coefficients. Noted that the only difference between these two parameter sets is the choice in background subtraction. Subtracting background 2, taken at the end of the measurement campaign, shows slightly greater agreement in the linear fit. Again, the 4.43% sample has the largest deviation from the fit. The R^2 coefficients for the 94/92 and 98/92 calibration equations are 0.985 and 0.972 respec-

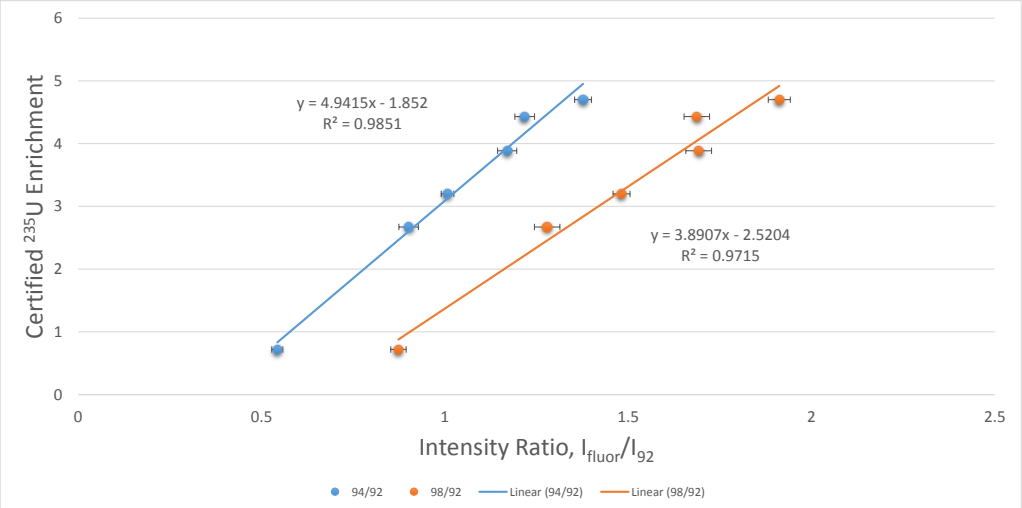

Figure 35: Intensity ratios 94.6 keV X-ray to 92* keV γ-ray and the 98.4 keV X-ray to 92* keV γ-ray plotted versus certified ^{235}U enrichment for parameter set 5. The linear fit to each set of data is shown with the associated fit equation and the R^2 coefficient.

tively. If the 4.43% sample were to be removed due to apparent defects in the measurement, the R^2 coefficients would increase to 0.993 and 0.988 respectively. These coefficients show strong agreement with a linear fit to the data. Lastly, the standard deviations associated with the ratio values are the smallest of all the parameter sets thus far.

Table 24: Peak area estimates from FRAM using parameter set 6 from Table 2 .

Declared (%)	92* Peak	94.6 keV Peak	98.4 keV Peak	94/92 Ratio	98/92 Ratio
0.72	1884	1042	1945	0.5531	1.0324
2.6725	1753	1709	2612	0.9749	1.4900
3.2	3906	4386	6707	1.1229	1.7171
3.8862	2818	3550	5577	1.2598	1.9791
4.4308	2604	3233	4755	1.2416	1.8260
4.7	4939	7222	11542	1.4622	2.3369

Table 25: Table containing the standard deviation for each of the three peaks used in the ratio method analysis as well as the standard deviations of the ratios themselves. Results refer to data processed using parameter set 6 from Table 2.

Declared (%)	σ_{92^*} (counts)	$\sigma_{94.6}$ (counts)	$\sigma_{98.4}$ (counts)	$\sigma_{94/92}$	$\sigma_{98/92}$
0.72	187	151	167	0.0214	0.0334
2.6725	128	166	167	0.0331	0.0460
3.2	246	216	239	0.0247	0.0346
3.8862	225	207	213	0.0318	0.0457
4.4308	172	158	163	0.0327	0.0445
4.7	280	271	272	0.0270	0.0397

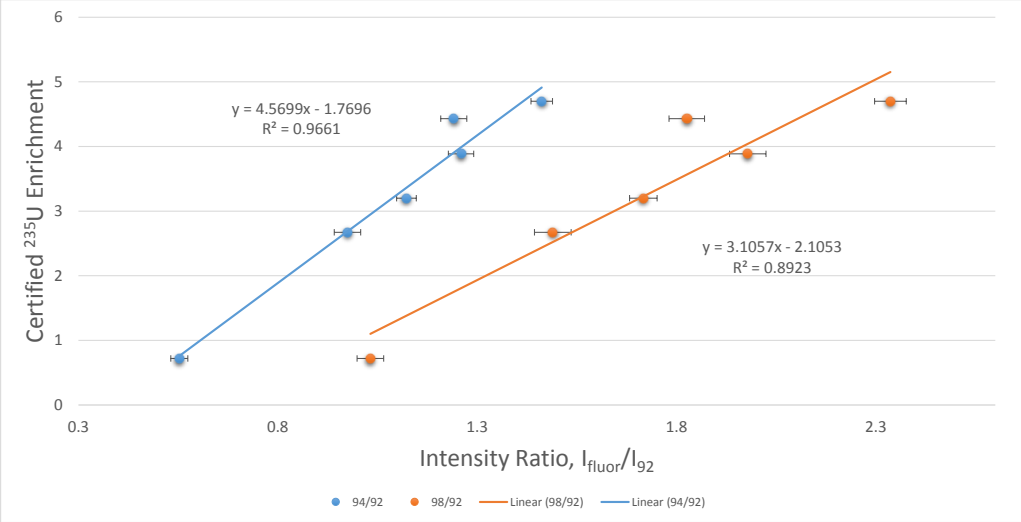

Figure 36: Intensity ratios 94.6 keV X-ray to 92* keV γ-ray and the 98.4 keV X-ray to 92* keV γ-ray plotted versus certified ^{235}U enrichment for parameter set 6. The linear fit to each set of data is shown with the associated fit equation and the R^2 coefficient.

Shown in Table 2, parameter sets 4-5 and parameter sets 6-7 only differ by the charge sharing algorithm used. The transition from CSA $\rightarrow$ to CSD should show a net decrease in photopeak counts, but overall be a less noisy spectrum. Comparing Table 20 to Table 24 we observe this to be true.

However, this decrease in net peak counts appears to have caused the standard deviations of the peak ratios to increase due to fewer counting statistics. Overall the fitted lines in Fig. 36 appear to be nominal, with R^2 coefficients of 0.966 and 0.892 for the 94/92 and 98/92 calibration equations respectively. Notably, the 98/92 R^2 coefficient has decreased by $\approx 10\%$. Again this is due to the 4.43% sample exhibiting unusual behavior. If this sample were to be removed from the analysis, the R^2 coefficients for the 94/92 and 98/92 calibration equations would increase to 0.999 and 0.974 respectively. An R^2 coefficient of 0.999 is ideal, it shows near-perfect correlation between the data and a linear fit.

Table 26: Peak area estimates from FRAM using parameter set 7 from Table 2 .

Declared (%)	92* Peak	94.6 keV Peak	98.4 keV Peak	94/92 Ratio	98/92 Ratio
0.72	2456	1427	2438	0.5810	0.9927
2.6725	1879	1858	2806	0.9888	1.4933
3.2	3725	4201	6435	1.1278	1.7275
3.8862	2348	3027	4531	1.2892	1.9297
4.4308	2580	3189	4644	1.2361	1.8000
4.7	4549	6702	10445	1.4733	2.2961

The results from parameter set 7 are very similar to those produced from parameter set 6. The R^2 coefficients for the 94/92 and 98/92 calibration equations are 0.956 and 0.901 respectively. Again, if the 4.43% sample is discluded due to its non-linearity, the R^2 coefficients increase to 0.999 and 0.984 respectively. This is a slight improvement over parameter set 6. Lastly, the standard deviations compare well with those observed in parameter set

Table 27: Table containing the standard deviation for each of the three peaks used in the ratio method analysis as well as the standard deviations of the ratios themselves. Results refer to data processed using parameter set 7 from Table 2.

Declared (%)	σ_{92^*} (counts)	$\sigma_{94.6}$ (counts)	$\sigma_{98.4}$ (counts)	$\sigma_{94/92}$	$\sigma_{98/92}$
0.72	223	165	162	0.0193	0.0284
2.6725	153	146	145	0.0324	0.0445
3.2	230	205	223	0.0254	0.0356
3.8862	173	159	163	0.0355	0.0491
4.4308	171	151	155	0.0327	0.0442
4.7	253	243	244	0.0283	0.0408

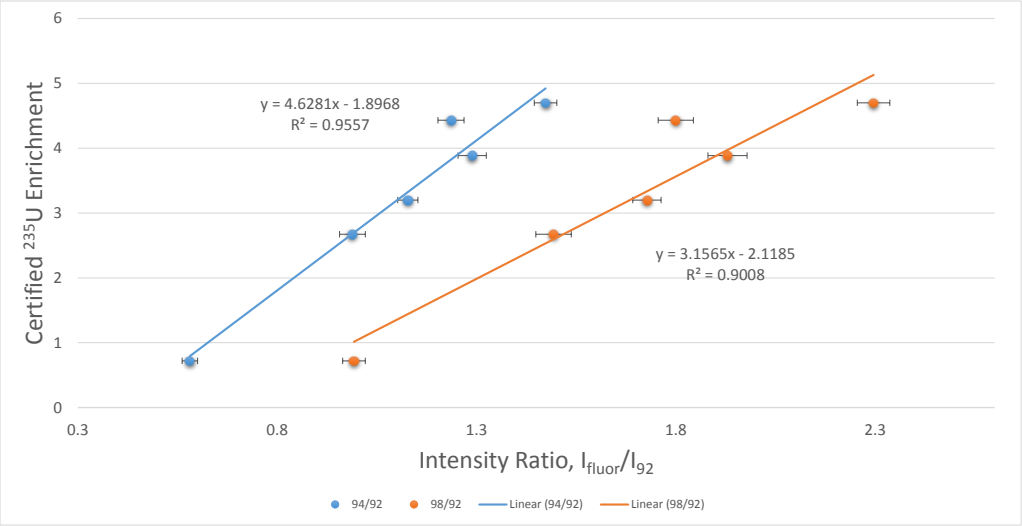

Figure 37: Intensity ratios 94.6 keV X-ray to 92* keV γ-ray and the 98.4 keV X-ray to 92* keV γ-ray plotted versus certified ^{235}U enrichment for parameter set 7. The linear fit to each set of data is shown with the associated fit equation and the R^2 coefficient.

6.

The ratio method demonstrates promise for accurate quantitative analysis of enriched uranium samples using the HEXITEC system. The performance of the method when analyzing the subsequent 2.80% sample is

shown in Table 32. Parameter sets 4 and 5 perform the best in both %Diff. and %RSD. Specifically, parameter set 4 calculated the ^{235}U enrichment to be $2.76 \pm 0.05\%$, while the expected value is 2.80%. The true value falls within the calculated range suggesting this method can be applied to a larger number of samples using parameter set 4.

Table 28: Estimates of the enrichment of the 2.80% sample, calculated using the calibration equations from the seven parameter sets. Additionally, the %RSD values are given for each parameter set.

Parameter Set	Calculated Enrichment	%Diff.	%RSD
1	2.99	6.93	2.34
2	3.32	18.59	3.12
3	3.32	18.70	2.69
4	2.76	-1.27	2.28
5	2.69	-3.97	2.16
6	1.92	-31.34	2.60
7	1.91	-31.84	2.57

Fig. 38 illuminates the ratio method's accuracy using the seven different parameter sets for this one sample. Two additional samples were measured to test the validity of the ratio method, however, a bug in the detector's software caused the samples to be unusable. Therefore, with one data point to validate the ratio method, it appears that parameter sets 1, 4 and 5 perform the best. Parameter set 1 has poor R^2 coefficients and is not considered for this reason. Parameter sets 4 and 5 have the best R^2 coefficients as well as the smallest standard deviations. Further, parameter set 4 is the only parameter set that contains the true value in its range from Fig. 38. For future measurements with unknown enrichment, parameter set

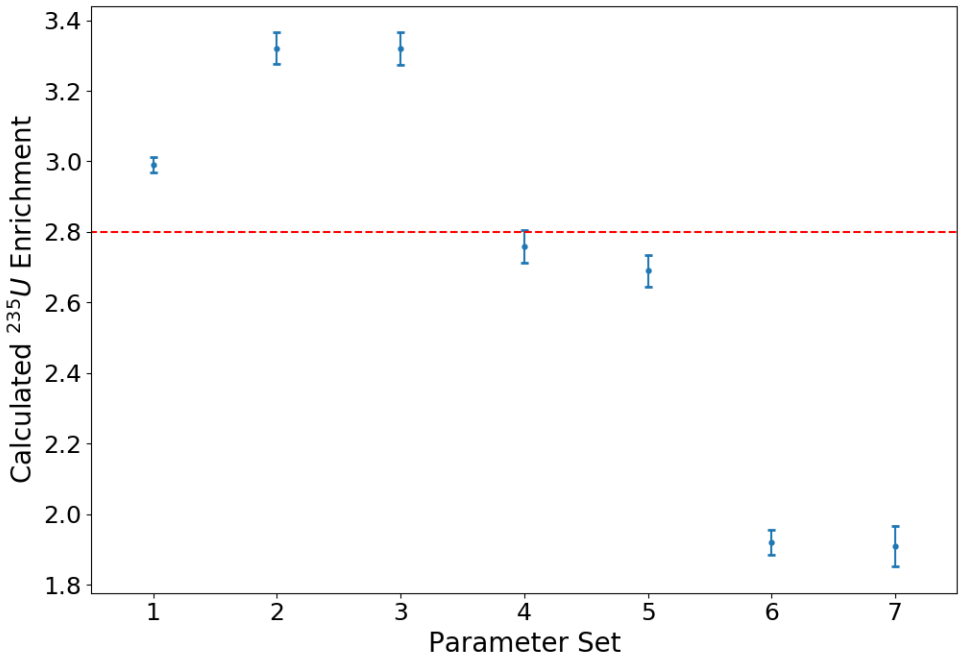

Figure 38: Plotted are the calculated enrichments of the 2.80% sample using the ratio method for each of the parameter sets listed in Table 2. The known reference value is plotted as a dashed red line. Each calculated value is plotted with its associated standard deviation.

4 is recommended in order to produce the most accurate results.

The two linear calibration equations created in the leave-out method only using the 0.72%, 3.2% and 4.7% enriched uranium samples and processed using parameter set 4 are shown in Fig. 39. With only three data points the R^2 values are quite good, as expected. Inserting the 94/92 and 98/92 peak ratios for the remaining four samples into their corresponding calibration equations yields a mean bias percentage of -9.59% and a %RSD value of 2.33%. The %RSD is calculated in the same manner that the IAEA does. Further, the %RSD value compares well to a ECGS system that performed a uranium enrichment analysis on U scrap using the MGAU approach, yielding

a %RSD value of 2.44.

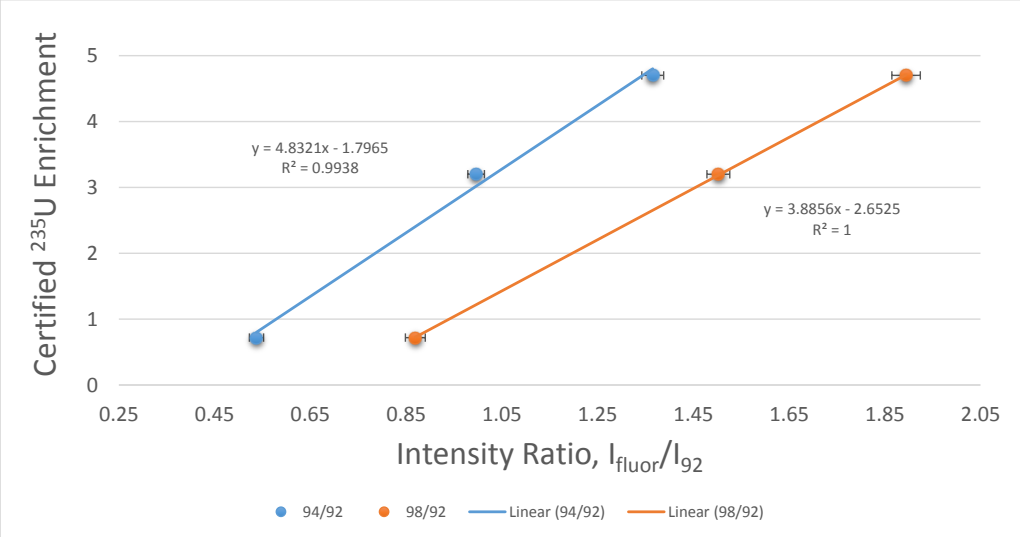

Figure 39: Intensity ratios 94.6 keV X-ray to 92* keV γ-ray and the 98.4 keV X-ray to 92* keV γ-ray plotted versus certified ^{235}U enrichment for the three selected samples. The linear fit to each set of data is shown with the associated fit equation and the R^2 coefficient

3.4 Modeling

3.4.1 Benchmarking

MCNP's Vised software is used to visualize the source/detector model as defined in MCNP. The 3-D isometric view of the modeled system with transparent features is shown in Fig. 40.

The simulated geometry (Fig. 40) accurately replicates the experimental system in Fig. 6, merely rotated. Next, the particle tracks were visualized to ensure the photon interactions are occurring where expected, again using Vised.

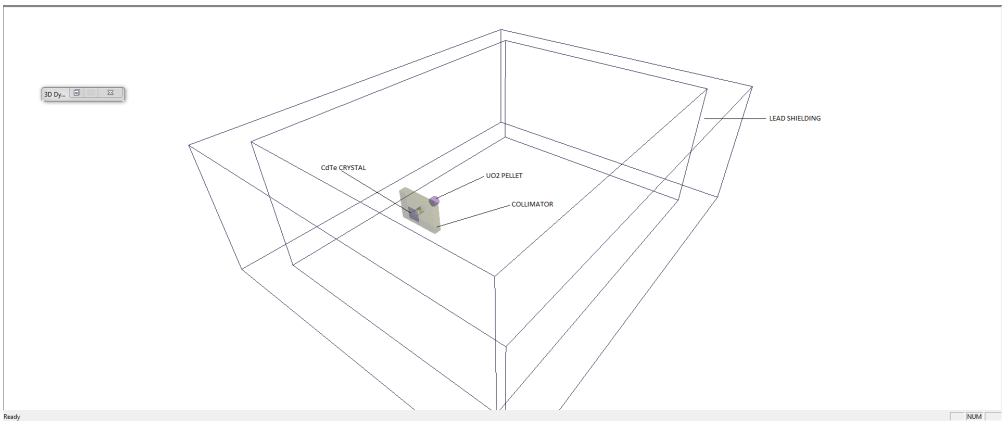

Figure 40: Shown is a 3-D isometric view of the transparent system modeled in MCNP6.2 with key components labeled.

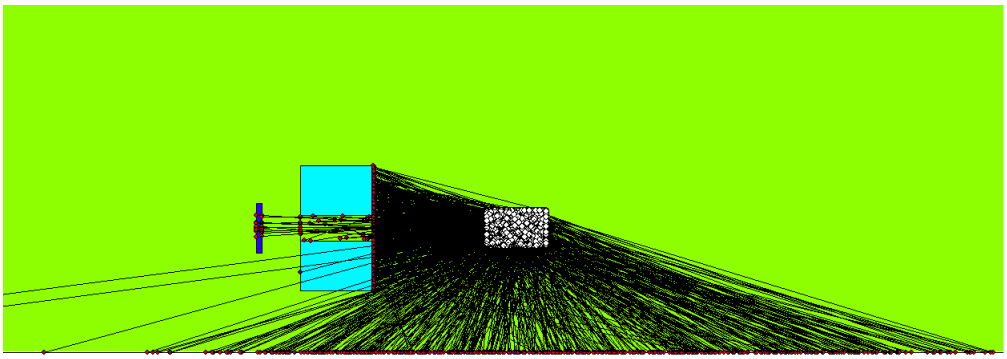

Figure 41: Shown is a 2-D view of the close-up HEXITEC system with 50,000 photon tracks simulated.

The majority of photons shown in Fig. 41 appear to interact with the collimator and lead shielding at the bottom edge nearest the sample. With 50,000 photons simulated, only about 15 interact with the detector. This helps to explain the need for longer acquisition times.

Plots of the measured data compared to the corresponding MCNP simulated data are shown in Figs. 42-44. Note, all modeled spectra have relative error, $R < 0.05$ for each peak in the UXK_{α} spectral region. As a

visual inspection, all three plots appear to have nominal peak areas. The MCNP predicted 98.4 keV peak is overestimated in both the 3.9% and 4.7% simulations. However, the 94.6 peak is predicted well with MCNP in the 3.9% and 4.7% ^{235}U samples, but underestimated in the 2.67% sample. The 92* peak is well-modeled in all three samples. The largest discrepancy between the data and the model comes from the differences in background.

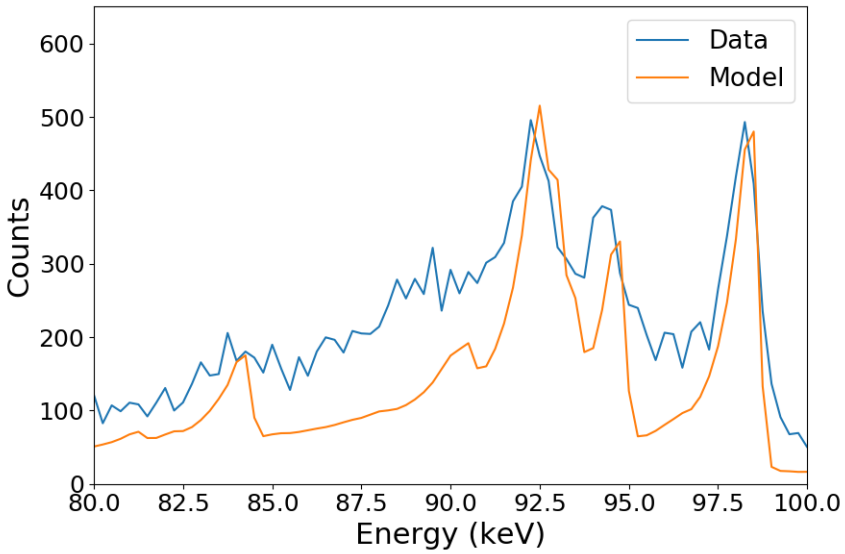

Figure 42: Plot of the measured vs modeled data for the 2.67% enriched sample.

The DRF was constructed in a way that attempted to mimic the CSD algorithm used in the SpecX system, whereas the enrichment data is processed using the CSA algorithm. The main difference observed in the CSD vs CSA algorithms is detailed in Section 3.1.2. In short, the CSA algorithm yields slightly higher peak counts, but an overall elevated tailing term and background. Figs. 42-44 show the hole-tailing and background as the largest

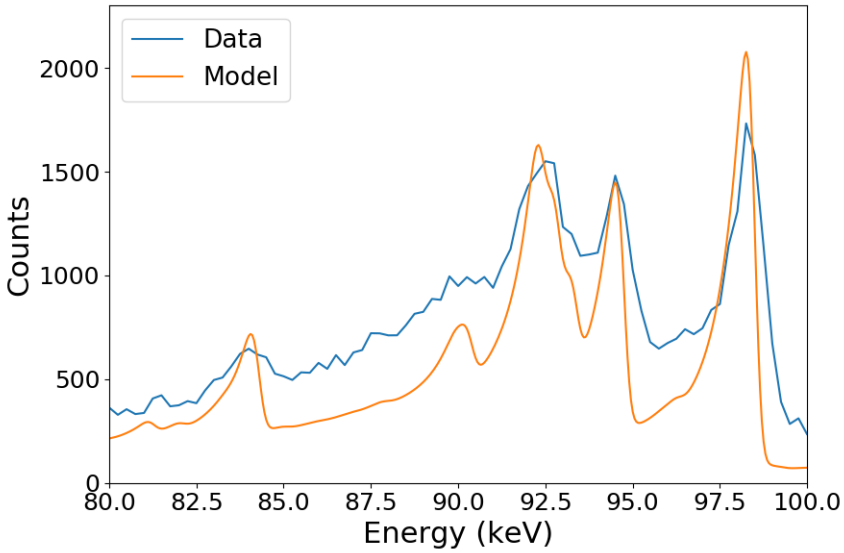

Figure 43: Plot of the measured vs modeled data for the 3.9% enriched sample.

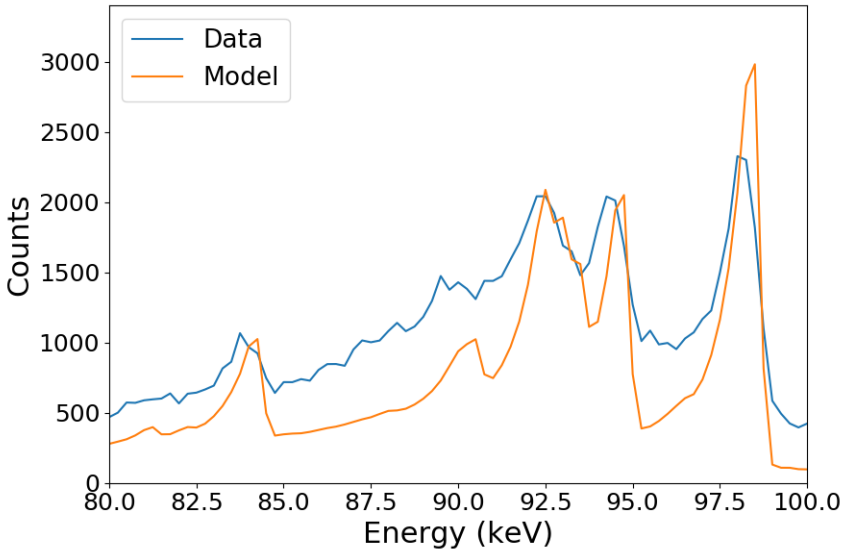

Figure 44: Plot of the measured vs modeled data for the 4.7% enriched sample.

discrepancy. Instead, the CSD vs model spectra are shown in Fig. 45.

Fig. 45 shows stronger agreement between the measured vs. modeled

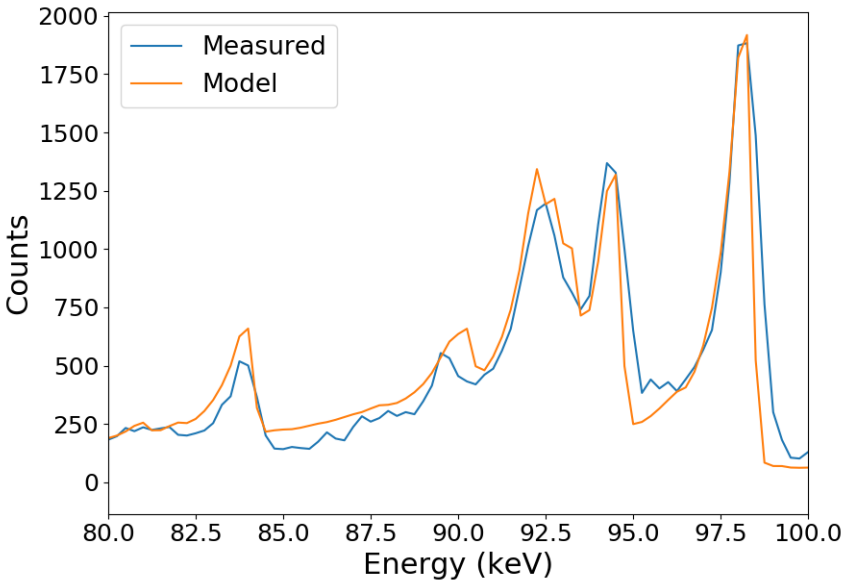

Figure 45: Plot of the CSD processed spectrum vs the MCNP generated spectrum of identical enrichment.

data in lieu of the spectra processed using the CSA approach. The tailing features along with the overall background match quite well. The goodness of fit between the model and data was quantified using the reduced chi-square value, χ^2_ν. The χ^2_ν values were calculated using Eq. 9, where ν is the degrees of freedom, O_i is the data at point i, C_i is the model at point i, and σ_i^2 is the standard deviation at point i.

$$\chi^2_\nu = \frac{1}{\nu}\sum_{n=1}^{N}\frac{(O_i - C_i)^2}{\sigma_i^2} \tag{9}$$

The χ^2_ν value for the 4.7% enriched sample using the CSA approach is 371. The χ^2_ν value for the same sample, but using the CSD approach is 42, nearly an order of magnitude smaller. In summation, the DRF and the MCNP input

deck are reasonably modeling the measured spectra, however the CSD approach shows better agreement. With this validated approach, future MCNP samples can be generated with enrichments beyond the scope of what is available to measure.

3.4.2 Generating Enriched Data

In total there are five MCNP-generated samples with enrichments 2.67%, 4.7%, 6.0%, 20.0%, and 60.0%. The 2.67% and 4.7% samples are generated to provide a comparison between the performance of the FRAM and Ratio methods on real measured samples versus modeled samples. Fig. 46 shows the 80-100 keV region of all five MCNP-generated spectra. As expected, as the ^{235}U enrichment increases, as do the contributions from the 93.35, 94.6 and 98.4 keV peaks.

The results from FRAM appear to become very inaccurate beyond 5% enrichment, as seen in Table 29. Notably, the 60% modeled sample is estimated to be 30%, half of the true value. However, the FRAM algorithm works at a nominal level for the 2.67% and 4.7% samples. Upon inspection, as the modeled enrichment increases, the FRAM fitting process increasingly underestimates the contributions from the 186 keV peak. This will lead to an overall underestimation in the sample enrichment, as observed in Table 29.

The peak areas in the UXK_α spectral region are taken from the FRAM fitting output for use in the ratio method. The calibration equations

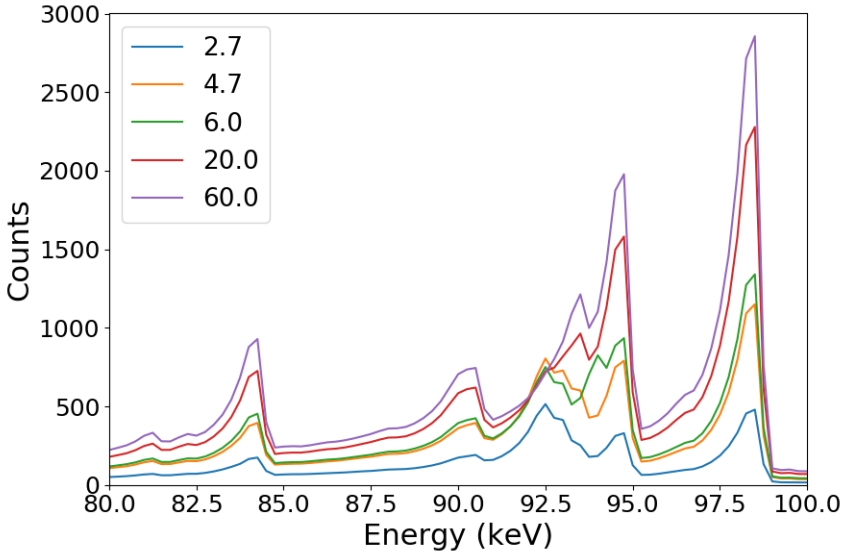

Figure 46: Plot of all five spectra generated in MCNP, showing only the 80-100 keV region.

Table 29: Contains the results from FRAM for the MCNP-generated spectra.

Known (%)	FRAM Calc. (%)	Measured-Declared	Sigma	%Diff.	%RSD
2.67	2.975	0.305	0.963	10.261	32.38
4.70	4.723	0.023	1.263	0.481	26.75
6.00	4.632	-1.368	1.377	-22.800	29.74
20.00	15.061	-4.940	6.066	-24.700	40.28
60.00	30.226	-29.774	19.925	-49.620	65.92

for the 94/92 and 98/92 peak ratios are taken from parameter set 4. The peak areas as well as ratio values are shown in Table 30.

The ratio method results show direct contrast to the FRAM method. In the FRAM method, the two lower enriched samples perform well, but the three higher enrichments are inaccurate. Whereas, in the ratio method the two lower enriched samples do not perform well while the three higher

Table 30: Contains the peak areas from the fit analysis in FRAM as well as the calculated peak ratios.

Declared (%)	92* Peak	94.6 keV Peak	98.4 keV Peak	94/92 Ratio	98/92 Ratio
2.67	2120	1254	1729	0.5915	0.8156
4.70	2907	3079	4123	1.0592	1.4183
6.0	2440	4353	4791	1.7840	1.9635
20.00	1373	6367	8170	4.6373	5.9505
60.00	694	8054	10294	11.6052	14.8329

Table 31: Contains the standard deviations of the quantities provided in Table 30 above.

Declared (%)	σ_{92^*} (counts)	$\sigma_{94.6}$ (counts)	$\sigma_{98.4}$ (counts)	$\sigma_{94/92}$	$\sigma_{98/92}$
2.67	327	242	233	0.021	0.026
4.70	503	432	416	0.027	0.034
6.00	490	483	443	0.045	0.049
20.00	596	651	626	0.138	0.174
60.00	645	753	728	0.459	0.582

Table 32: Contains the results from the Ratio method for the MCNP-generated samples, using the calibration equations from parameter set 4.

Known Enrichment	Calculated Enrichment	%Diff.	%RSD
2.67	0.905	-66.12	11.82
4.70	3.273	-30.37	4.24
6.00	6.160	2.66	3.43
20.00	21.232	6.16	3.30
60.00	56.319	-6.13	4.16

enrichments are nominal. The mean %Diff. is 21.57 and 22.29 for the FRAM and ratio method respectively. The mean %RSD is 39.01 and 5.39 for the FRAM and ratio method respectively. The percent differences between the methods are similar, but the ratio method performs much better in terms of

percent RSD.

4 Conclusions and Future Work

4.1 Analysis of Results

The research presented explored the ability for the SpecX system's HEXITEC CdTe detector to accurately measure sample ^{235}U enrichment. There were three methods used for comparison; the FRAM method, the Ratio method and the GEM method. A model was created that was used to help understand the detector response and source emissions, With a known detector response, synthetic spectra of samples not measured were then generated.

There were a total of seven parameter sets used for processing the six uranium samples. Each set of processed data was analyzed in FRAM to determine the best performing parameter set. It was found that parameter set 5, in which the CSA approach was used in combination with an ROI selection, performed the best in terms of accuracy and precision. Further, the four samples with enrichments ranging 0.72%-3.2% and processed using parameter set 5 deviated from their known enrichments by an average of $0.044 \pm 0.016\%$. While the small deviations are encouraging, the large %RSDs are not. In parameter set 5, the average %RSD for all six samples is 35.6%. While this reporting of %RSD is different than that of the IAEA, this does not detract from the fact that these values of %RSD are far too large to produce consistent results. Thus, the performance of the HEXITEC

detector while using FRAM does suit the precision standards required for IAEA measurements.

Similar to the FRAM method, the Ratio method was tested on all seven parameter sets. For each parameter set, two calibration lines were constructed for the 94/92 and 98/92 peak ratios. The calibration lines were judged based on their R^2 coefficients.

Parameter sets 4 and 5 showed the best goodness of fits, while maintaining the smallest %RSDs. Further, when each of the seven sets of calibration lines were applied to a subsequently measured sample, parameter set 5 deviated from the known enrichment by -3.97%. However, parameter set 4 was the most accurate with a percent difference of -1.27% accompanied by a %RSD of 2.28. Again, this method of %RSD differs from the reported IAEA %RSD. The true sample enrichment was 2.80%, while parameter set 4 estimated the ^{235}U enrichment to be $2.76 \pm 0.05\%$. These results are a stark improvement to those derived from the FRAM method. More samples would need to be measured to test the method's repeatability. Lastly, the leave-out method used with the Ratio method was able to produce a %RSD value of 2.33, which is generated in the same fashion as the IAEA. This value compared quite well to the ECGS system's %RSD value of 2.44. With these factors in consideration, the Ratio method shows promise.

The GEM method encountered several difficulties. Without a user manual and the lack of ability to adjust fitting parameters, the quality of fit on all input spectra was quite poor. Further, only the calibration file with

enrichment 4.7% and the sample of enrichment 2.67% were able to produce any results. The remaining four spectra yielded calculations of "infinity" enrichment, which is illogical. If more time were allotted towards this method, working with the method's developers could produce meaningful results.

The experimental data was validated against a MCNP6.2 model with a subsequently applied DRF. Each peak within the UXK_α spectral region maintained a relative error $R < 0.05$. The modeled spectra performed nominally when compared to the CSA processed data. However, the modeled spectra show greater agreement to the CSD processed data, as this was the intended purpose of the DRF.

New spectra were then generated in MCNP with ^{235}U enrichment beyond the scope of what was available to measure. These new spectra were analyzed using the FRAM and Ratio methods. The FRAM method accurately analyzed low-enrichment MCNP spectra, but was unable to determine the enrichment of spectra with ^{235}U content $\geq$ 6.0%. The Ratio method incorrectly predicted the lowly-enriched spectra, but showed superior performance when analyzing the spectra with higher enrichment.

In summation, the HEXITEC CdTe detector has shown promise in its ability to accurately and non-destructively estimate ^{235}U sample enrichment using either the FRAM or Ratio method. In order to effectively use FRAM, the issues involving the 186 keV peak would likely need to be resolved. The Ratio method showed that it was able to correctly calculate the 2.80% sample's enrichment within 1σ. Further samples would need to

be measured and analyzed using the Ratio method to confirm the accuracy. The GEM method was unable to calibrate upon our poor 186 keV photopeak. Without resolving this detector issue, the GEM method is not a valid approach.

4.2 Future Work

Moving forward there are an assortment of new tests that could be ran with time permitted. First, new enrichment samples are needed to test the repeatability of the Ratio method under parameter set 4. Second, a custom spectrum de-convolution process should be created for finer control over fitting parameters. This should improve the results consistency as the process will be catered specifically to the HEXITEC detector. Third, a deep dive into the issues with the 186 keV peak may allow for more accurate use of the GEM and FRAM methods. Lastly, a windowed collimator can be designed to determine if enrichment measurements based on regions of the detector are possible using the HEXITEC's pixelated response.

References

[1] Gilbert, Andrew J., et al. *"Non-Invasive Material Discrimination Using Spectral X-ray Radiography."* Journal of Applied Physics, vol. 115, no. 15, 2014, p. 154901., doi:10.1063/1.4870043.

[2] "Non-Proliferation Treaty." IAEA, IAEA, 8 June 2016, www.iaea.org/topics/non-proliferation-treaty. Accessed 22 Feb. 2019.

[3] *"Treaty Verification: Understanding IAEA Safeguards."* Nuclear Threat Initiative, tutorials.nti.org/nonproliferation-regime-tutorial/treaty-verification-understanding-iaea-safeguards/. Accessed 22 Feb. 2019.

[4] *"Additional Protocol."* IAEA, IAEA, 8 June 2016, www.iaea.org/topics/additional-protocol. Accessed 22 Feb. 2019.

[5] *"Safeguards in Practice."* IAEA, IAEA, 8 June 2016, www.iaea.org/topics/safeguards-in-practice. Accessed 22 Feb. 2019.

[6] McDonald, Benjamin, et al. *"Determining uranium mass in powder samples with spectral radiography."* Symposium on International Safegaurds, Vienna, 2018.

[7] Berlizov, Andrey, et al. *"Feedback from operational experience of on-site deployment of bias defect analysis with COMPUCEA."* Journal of Radioanalytical and Nuclear Chemistry 307.3 (2016): 1901-1909.

[8] Zhao, K., et al. *"International target values 2010 for measurement uncertainties in safeguarding nuclear materials."* ESARDA Bulletin 48 (2012): 3-24.

[9] Ottmar, H., et al. *"Uranium Enrichment Assay with a LaBr3(Ce) Scintillation Detector: A Promising Option for the 2nd Generation of COMPUCEA"*. ESARDA Bulletin, 32-39.

[10] Mortreau, Patricia, and Reinhard Berndt. *"Determination of the uranium enrichment with the NaIGEM code."* Nuclear Instruments and Methods in Physics Research Section A: Accelerators, Spectrometers, Detectors and Associated Equipment 530.3 (2004): 559-567.

[11] Gunnink, R. *"A Guide for Using NaIGEM, PC Version 1.51 b for DOS and Windows." (2002).*

[12] A. J. Gilbert, B. S. McDonald, and L. E. Smith. "Spectral X-ray Radiography for Safeguards at Nuclear Fuel Fabrication Facilities: A Feasibility Study", in *International Conference on Mathematics & Computational Methods Applied to Nuclear Science & Engineering*, Jeju, Korea, 2017: Korean Nuclear Society.

[13] *"X-ray Edge Energies."* DATA COMPRESSION: ADVANTAGES AND DISADVANTAGES, 9 Jan. 2017, www.esrf.eu/UsersAndScience/Experiments/StructMaterials/ID11/ID11UserGuide/ID11Edges.

[14] Ottmar, Herbert, et al. *"Uranium Enrichment Assay with a LaBr 3 (Ce) Scintillation Detector: A Promising Option for the 2 nd Generation of COMPUCEA."* ESARDA Bulletin 38 (2008): 32-39.

[15] Vo, Duc T., and Thomas E. Sampson. *Uranium isotopic analysis with the FRAM isotopic analysis code*. No. LA–13580. Los Alamos National Lab., 1999.

[16] Gunnink, R., et al. *"MGAU: A new analysis code for measuring uranium-235 enrichments in arbitrary samples."* International nuclear safeguards 1994: Vision for the future. V. 2. Proceedings of a symposium held in Vienna, 14-18 March 1994. 1994.

[17] Korob, R. O., and GA Blasiyh Nuño. *"A simple method for the absolute determination of uranium enrichment by high-resolution γ spectrometry."* Applied radiation and Isotopes 64.5 (2006): 525-531.

[18] Yücel, H., and H. Dikmen. *"Uranium enrichment measurements using the intensity ratios of self-fluorescence X-rays to 92* keV gamma ray in UXK_α spectral region."* Talanta 78.2 (2009): 410-417.

[19] Abbas, K., et al. *"Use of miniature CdZnTe X/γ detector in nuclear safeguards: Characterization of spent nuclear fuel and uranium enrichment determination."* Nuclear Instruments and Methods in Physics Research Section A: Accelerators, Spectrometers, Detectors and Associated Equipment 405.1 (1998): 153-158.

[20] Brodsky, S. M. *"Application of CdTe Detector for Determining Uranium Enrichment on 89–100 keV γ-and X-ray Radiation."* Atomic Energy 114.6 (2013): 421-427.

[21] Veale, M. C., et al. *"Measurements of charge sharing in small pixel CdTe detectors."* Nuclear Instruments and Methods in Physics Research Section A: Accelerators, Spectrometers, Detectors and Associated Equipment 767 (2014): 218-226.

[22] Baumgartner, Wayne H., et al. *"The HEXITEC hard X-ray pixelated CdTe imager for fast solar observations."* High Energy, Optical, and Infrared Detectors for Astronomy VII. Vol. 9915. International Society for Optics and Photonics, 2016.

[23] *"Scipy.signal.ricker."* Scipy.stats.trim_mean - SciPy v1.1.0 Reference Guide, docs.scipy.org/doc/scipy-0.13.0/reference/generated/scipy.signal.ricker.html.

[24] Ed S.A. (Ed.), *Solid-State Radiation Detectors Technology and Applications.* Devices, Circuits, and Systems, CRC Press, Boca Raton, FL (2015), p. 384

[25] Wilson, M. D., et al. *"A 10 cm× 10 cm CdTe spectroscopic imaging detector based on the HEXITEC ASIC."* Journal of Instrumentation 10.10 (2015): P10011.

[26] Nakagawa, Hisaya, et al. *"Carrier Transport Properties of CdTe Detector under Polarization Condition."* Sensors and Materials 30.7 (2018): 1605-1610.

[27] Sampson, Thomas E., Thomas A. Kelley, and Duc T. Vo. *"Application guide to gamma-ray isotopic analysis using the FRAM software."* Los Alamos National Laboratory document LA-14018 (2003).

[28] Goorley, T., et al., *Initial MCNP6 release overview*. Nuclear Technology, 2012. 180(3): p. 298-315.

A MCNP Input File

```
C ---- MCNP HEXITEC Enrichment Model ------
C =======+++CELL DEFINITIONS+++============
C
C CdTe Detector
1 200 -6.2      -1       imp:n=1 imp:p=1  $ cell for CdTe crystal
2 300 -19.3     -2 3      imp:n=1 imp:p=1  $ W block cell
3 500 -11.35    -5 4         imp:n=1 imp:p=1  $ Pb Shielding
4 400 -0.001205 -4 1 2 3 6   imp:n=1 imp:p=1  $ Fill Vol w/Air
5 400 -0.001205 -3       imp:n=1 imp:p=1  $ Air in Coll. hole
6 600 -10.597 -6       imp:n=1 imp:p=1  $ UO2 pellet
999    0    5           imp:n=0 imp:p=0  $ void

c +++SURFACE DEFINITIONS+++================
C ------------------------
1 rpp -0.1 0 -1 1 -1 1                      $ CdTe crystal
C                                             2 cm x 2 cm x 1 mm
2 rpp 0.65 1.90 -3.5 3.5 -2.5 2.5           $ W collimator block
C                                             5cm x 7cm x 1.25cm
3 rcc 0.65 0 0 1.25 0 0 0.5                 $ Hole of collimator
C                                             of 1 cm diameter
4 rpp -15.24 35.56 -27.94 10.16 -5 15.32    $ Inner RPP of Pb
```

```
5 rpp -20.32 40.64 -33.02 15.24  -5 15.32   $ Outer RPP of Pb
6 rcc 3.825 0 0 1 0 0 0.715                 $ UO2 Fuel pellet


C Data cards
m200  52000.04p -0.531645       $ CdTe Detector-quality
      48000.04p -0.468355
m300  74000 1                   $ standard tungsten
m400                            $ Air [NIST]
      6000  -0.000150
      7014  -0.784431
      8016  -0.210748
      18000 -0.004671
m500  82000 1                 $ Pb
m600                          $   Uranium 4.7% enriched U-235
      8016       4.7287e-02     $ O_2
      92234.03p  1.0504e-04     $ U-234
      92235.03p  1.1248e-03     $ U-235
      92238.03p  2.2508e-02     $ U-238
C Source Cards
mode p
print 110
RAND STRIDE = 1000
nps 5e9
```

```
C
SDEF  x=d1  y=d2  z=d3  PAR=2  ERG=d6 CEL=6
si1 3.825 4.825
sp1 0 1
si2 -.715 .715
sp2 0 1
si3 -.715 .715
sp3 0 1
#    si6        sp6
        l         D
            o
            o
            o
F8:P  1
e8 0 1e-5 0.25e-3 1198i 0.3
```